

**An improved organ explant culture method reveals stem cell lineage dynamics in the adult *Drosophila* intestine**

**Marco Marchetti, Chenge Zhang, and Bruce A. Edgar**

Department of Oncological Sciences, Huntsman Cancer Institute, University of Utah, Salt Lake City, UT 84112, USA

Correspondence and requests for materials should be addressed to B.A.E. (email: bruce.edgar@hci.utah.edu)

**Keywords:** *Drosophila* midgut, organ culture, live-imaging, tissue regeneration, cell lineage, cell fate, stem cells.

**Abstract:** In recent years, live-imaging techniques have been developed for the adult midgut of *Drosophila melanogaster* that allow temporal characterization of key processes involved in stem cell and tissue homeostasis. However, these organ culture techniques have been limited to imaging sessions of  $\leq 16$  hours, an interval too short to track dynamic processes such as damage responses and regeneration, which can unfold over several days. Therefore, we developed an organ explant culture protocol capable of sustaining midguts *ex vivo* for up to 3 days. This was made possible by the formulation of a culture medium specifically designed for adult *Drosophila* tissues with an increased  $\text{Na}^+/\text{K}^+$  ratio and trehalose concentration, and by placing midguts at an air-liquid interface for enhanced oxygenation. We show that midgut progenitor cells can respond to gut epithelial damage *ex vivo*, proliferating and differentiating to replace lost cells, but are quiescent in healthy intestines. Using *ex vivo* gene induction to promote stem cell proliferation using *Ras*<sup>G12V</sup> or *string* and *Cyclin E* overexpression, we demonstrate that progenitor cell lineages can be traced through multiple cell divisions using live imaging. We show that the same culture set-up is useful for imaging adult renal tubules and ovaries for up to 3 days and hearts for up to 10 days. By enabling both long-term imaging and real-time *ex vivo* gene manipulation, our simple culture protocol provides a powerful tool for studies of epithelial biology and cell lineage behavior.

## INTRODUCTION

Endo- and ectodermal epithelia comprise essential interfaces between an organism and its environment. As such, they form a first line of defense that is frequently subjected to diverse types of insult. This situation requires that epithelia be able to mount appropriate responses. This is possible in part due to the action of resident stem cells which, through their ability to self-renew and produce differentiated progeny, allow epithelia to regenerate both structurally and functionally. The adult *Drosophila melanogaster* midgut is a prime example of this as its population of intestinal stem cells (ISCs) are able to interpret signals from their surrounding environment such as cytokines released by neighboring damaged enterocytes (EC)<sup>1-5</sup>. When this interaction occurs, normally quiescent stem cells rapidly respond to the needs of the tissue, proliferating and stimulating the differentiation of their progeny to replace lost cells, thus repairing the damaged epithelium<sup>3,5</sup>.

The understanding of epithelial biology has been greatly advanced by protocols for the *ex vivo* culture and imaging of tissues and organs. For example, mammalian intestinal organoids have advanced the field by easily allowing the direct observation of stem cell behavior, without the need for intravital imaging<sup>6</sup>. Several protocols have been developed for the live-imaging of *Drosophila* tissues and organs such as imaginal discs<sup>7-11</sup>, larval brains<sup>12,13</sup>, ovaries<sup>14-16</sup>, testis<sup>17</sup> and, more recently, adult midguts<sup>18-22</sup>. The small size of fruit flies makes it possible to culture whole intact organs.

However, in contrast to mammalian tissues, many of which are easily cultured for long periods, most *Drosophila* organ cultures are limited in time to less than a day. This reflects an incomplete understanding of the culture conditions required to fully sustain explanted *Drosophila* tissues. Current approaches for the live-imaging of the fly midgut are limited to 16h of imaging due to the poor survival of explanted tissues<sup>21,22</sup>. Moreover, temperature-sensitive gene expression, knock-down, and knock



outs, some of *Drosophila* genetics strongest assets, cannot currently be implemented in combination with extended live-imaging because the elevated temperature further limits tissue viability<sup>21</sup>.

To address these limitations, we developed an improved *ex vivo* culture system for the live-imaging of adult *Drosophila* midguts. Our culture system employs a novel tissue culture medium tailored to the needs of adult *Drosophila* cells and organs, and culture at an air-media interface to ensure optimal oxygenation. The technique has a straightforward design, allowing multiple samples to be prepared quickly and reproducibly. The setup allows the researcher to image up to 12 midguts simultaneously during live-imaging sessions of 48-72h. As the guts are fully explanted from the animal, every region of the organ is clearly available for imaging, thus expanding the number of questions that can be addressed. We show that, while in healthy explanted intestines progenitor cells are quiescent, midguts can still respond to damage *ex vivo*, with progenitors proliferating and differentiating in response to tissue damage. Our protocol can also be used in conjunction with temperature-sensitive gene expression or knock-down. We demonstrate this by genetically driving progenitor cell proliferation. Moreover, due to the extended live-imaging window our protocol allows, we were able to follow cells undergoing multiple rounds of mitosis. By combining a long 48-72h imaging window and the possibility to use advanced *Drosophila* genetic tools, we provide a useful tool to probe and understand the biology of epithelial tissues.

## RESULTS

### A system for the long-term culture of adult *Drosophila* midguts

Current live-imaging protocols for the adult *Drosophila* midgut are limited to 16h imaging sessions<sup>18-22</sup>.

To extend the survival of midguts *ex vivo* we developed a novel culture setup. The method is based on common available techniques for the culture of adult organs<sup>6,9,16,22</sup> but it includes a refinement of several steps: 1) the dissection procedure was optimized to reduce tissue damage; 2) explanted organs

are cultured in a sandwiched structure of agarose, rather than in a dome; 3) midguts are placed at a liquid-air interface for improved oxygenation; 4) the culture media has been adjusted to better approximate adult hemolymph. Please see the Methods section step-by-step descriptions of the procedure.

We found that the dissection technique is a key parameter in extending the viability of explanted midguts. Indeed, any stress (*e.g.* pulling and thus stretching the gut, pinching, etc...) introduced during dissection results in structural damage which lead to breaks of the epithelium during prolonged culture. Hence, we have optimized the dissection procedure to limit the handling of the midgut and thus the risk of damaging it (Figure 1A-N and Video 1).

A key element of our system is enveloping explanted organs in a sandwich of low-melt agarose (Figure 1O). Immobilization in gels is a common solution for *ex vivo* culture of organs and tissues, and is especially important to provide stability for live-imaging applications<sup>6,9,16,22</sup>. For the adult *Drosophila* midgut specifically, an agarose gel also minimizes the effects of peristaltic movements, which, if uncontrolled, will impair imaging and can lead to epithelial tearing. Our approach is a slight departure from previously published techniques for *Drosophila* tissues<sup>9,16,22</sup> in that explanted midguts are transferred to evenly spaced thin agarose pads and then covered with an additional layer of agarose (Figure 1O). This sandwiched structure allows the guts to be held in place for imaging, while also protecting them from damage that can result from their contact with the culture chamber walls if left freely floating. The agarose pads can be reproducibly cast and are thin enough (~100µm) not to interfere with imaging. Moreover, each agarose pad can comfortably house up to 3 midguts, allowing the multiple imaging of several explanted intestines. The agarose pads have the additional function of elevating the midguts from the bottom of the imaging chamber so that the surface of the agarose structure is directly exposed to air, creating an air-liquid interface. This is a key design element of the setup, as proper oxygenation was found to be essential for the long-term survival of explanted midguts (data not shown),

similarly to what had been previously observed for the culture of wing imaginal discs<sup>11</sup>. Moreover, during dissection the trachea surrounding the intestine are severed and can no longer oxygenate the intestinal epithelium.

To increase the stability of the setup, agarose bridges connect each agarose sandwich (Figure 1O, middle panel), allowing the sample to endure 3 days of continuous imaging (Figure 2C and Video 2). Moreover, using a microscope equipped with an incubation chamber to control evaporation removes the need to replenish the imaging vessel with fresh culture medium. As such, the culture system, despite its simple design, is highly efficient and well suited for long-term imaging experiments.

#### **A culture medium tailored to adult *Drosophila* tissues enhances the survival of explanted midguts**

One of the factors currently limiting the extended survival of explanted adult *Drosophila* tissues is the lack of culture media specifically designed for this task. To obviate this issue, we analyzed several parameters that distinguish the hemolymph of larvae, on which most current *Drosophila* cell culture media are based, to that of adult flies. We therefore compared the performance of different media formulations using the incorporation *ex vivo* of the cell-impermeable dye NucGreen (Thermofisher) as a measure of cell death (Figure 2A). The dye was added at the start of the culture, and its accumulation in the tissue measured over the course of three days. At the start of the culture, we usually observed NucGreen incorporation only in trachea, which are inevitably severed and damaged as a result of the dissection. We found that raising the concentration of trehalose, which is found at high levels in *Drosophila* circulation<sup>23–27</sup>, and mimicking the Na<sup>+</sup>/K<sup>+</sup> ratio of adult hemolymph<sup>28–32</sup> is sufficient to significantly reduce cell death after 24h of culture. As Schneider's medium<sup>33–36</sup> is a common solution for several published protocols for the live-imaging of adult *Drosophila* tissues<sup>14,16,17,19,21</sup>, we modified it to raise the trehalose concentration to 50mM and Na<sup>+</sup>/K<sup>+</sup> ratio to levels similar to those found in adult *Drosophila* hemolymph (Table 1)<sup>24–26,28–32</sup>. Our tests showed that supplementing the culture medium

with 10% fetal bovine serum (FBS) did not have a significant beneficial effect on the midgut epithelium (Figure 2A), but we did notice that FBS addition resulted in the visceral muscle remaining intact and capable of peristalsis for longer (data not shown). Not surprisingly<sup>37,38</sup>, co-culturing explanted midguts with ovaries and abdomens lined with fat body (adipocytes) could also decrease cell death *ex vivo*. This effect was not due to the sequestration of NucGreen by ovaries and adipocytes as the dye was supplemented at a saturating concentration and its incorporation in these organs/tissues was mostly limited to areas mechanically damaged during dissection. As ovaries and fat bodies may enhance the survival of explanted midguts by secreting growth factors and/or nutrients, we reasoned that fly extract might have a similar effect. Indeed, midguts cultured in 100% fly extract prepared using modified Schneider's medium had greatly reduced rates of cell death over time (Figure 2A). The calcium blocker isradipine was also added to the medium to reduce peristaltic movements, improving midgut survival and imaging. This drug did not have a noticeable long-term effect on visceral muscle viability. Indeed, its effect appeared to wear off after 48-72h, at which point the visceral muscle resumed regular peristalsis (Video 3). Lastly, as we designed the medium for the purpose of extended live-imaging, we also added N-acetyl cysteine and sodium citrate as antioxidant agents to reduce phototoxicity<sup>39</sup>. The former is an antioxidant widely used in cell culture<sup>40</sup>. Citrate is also known to have antioxidant properties<sup>41</sup> and to be present in *Drosophila* hemolymph at detectable levels<sup>42</sup>. Combining all the findings mentioned above resulted in culture conditions (see Methods) that minimized cell death and allowed the live-imaging of explanted midguts for up to three days (Figure 2C and Video 2), a significant improvement over previously published culture protocols for the midgut in which imaging was limited to 16h<sup>21,22</sup>.

We successfully imaged cultured intestines with inverted microscopes of different kinds, including widefield (Nikon TiE), scanning confocal (Leica SP8), and lattice lightsheet (Zeiss LLS7). We did not notice signs of phototoxicity with any of these microscope types in samples imaged for 48h, but acquisition parameters had to be chosen with care. For example, by optimizing laser power and dwell time, single

intestines could be imaged at high frame-rates (15min) without noticeable phototoxicity for at least 48h even with a confocal microscope (Video 23). However, we found confocal imaging to be less optimal than widefield microscopy for high frame-rate imaging due to the longer acquisition time required for multiple midguts in a single sample.

In examining cultured midguts, we observed the accumulation of luminal contents (*i.e.* previously ingested food) in the posterior midgut (Figure 2B, white arrows). This appeared to be caused by peristaltic movements of the visceral muscle which persisted despite the use of the calcium blocker isradipine, although this drug suppressed them significantly. These areas were found to darken and expand over the course of culture, an effect we attribute to the growth of enteric bacteria, which eventually caused cell death and tissue damage. We found that feeding flies fresh food in the days prior to an experiment and a short (~3-6h) starvation prior to dissection reduced the negative effect of food accumulation and growth of enteric bacteria. Supplementing the culture medium with antibiotics also enhanced explanted midgut survival. Lastly, it is reasonable to assume that axenically reared flies should be immune to the issue of growing enteric bacteria.

### **Transgenic gene expression in midgut explant culture**

One of the most striking features of *Drosophila melanogaster* as a research model is the wide range of readily available genetic tools, allowing the cell-type-specific and temporally-controlled activation or suppression of expression of genes of interest. The possibility to use such genetic tools in a live-imaging setup is highly advantageous, but so far the temporal control of gene expression *ex vivo* has proven unfeasible<sup>21</sup>. To further assay the behavior of midgut cells in explanted organs, we tested the induction of UAS-GFP by cell type-specific, temperature-sensitive Gal4 drivers (Figure 2D-E)<sup>43,44</sup>. As expected, midguts explanted from flies grown at the restrictive temperature (18°C) did not show any GFP expression (Video 13 and Figure 2 – figure supplement 1A, left panels). However, when incubated at the

permissive temperature (29°C) at 0h after explant (Video 13 and Figure 2 – figure supplement 1A, right panels), they started expressing the UAS-GFP transgene. Moreover, GFP expression could also be induced in intestines cultured at 18°C for 24h and then shifted to the permissive temperature (29°C), indicating that the epithelium remains viable and genetically functional long-term (Figure 2 – figure supplement 1B). Indeed, the GFP intensity in midguts cultured at 29°C for 24h from the time of dissection was similar between *in vivo* and *ex vivo* conditions for both progenitor cells (Figure 2D) and enterocytes (Figure 2E) using the *escargot- (esg)* and *mex-Gal4 Gal80<sup>TS</sup>* driver lines, respectively. This indicates that transcription and protein synthesis are maintained at normal levels in our culture system and shows that this system can be used to assay the effects of transgene induction in real time. Interestingly, progenitor cells were found to be asynchronous in their expression of the reporter GFP (Fig 4A and Video 13). Usually, the first GFP+ cells were detected at 8-10h after temperature shift, though some cells achieved detectable GFP levels only 20 hours after that. Overall, if the shift to 29°C coincided with the start of imaging, all progenitor cells usually expressed detectable levels of GFP by the 36h time-point. This could be explained by variations in the activity of the *esg* promoter or by different global rates of transcription and translation, which in turn could be indicative of different cell states.

### **Progenitor cells require stimulation to proliferate and differentiate**

When imaging explanted adult *Drosophila* midguts we observed *esg*-expressing progenitor cells (ISCs and EBS) to be quiescent (Figure 3A and Videos 2, 4, and 7). Progenitor cells in explanted healthy guts did not show major changes in their GFP levels, indicative of continuous *esg* expression, nor in their nuclear size (Fig 3D,F,G and Video 7), which indicates that DNA content remains constant. Via cell tracking we also observed that GFP-labeled progenitor cells did not divide in healthy explanted intestines (Figure 4D). It is important to note that in said healthy intestines we did not observe cell death or enterocyte (EC) extrusion events until after 48-72h of culture. As healthy enterocytes are known to

suppress ISC proliferation<sup>45</sup>, this may explain the lack of cell division in our explants. The suppression of peristaltic movements by isradipine may also prevent EC loss by reducing mechanical tissue stress<sup>46</sup>.

A key feature of *Drosophila* intestinal progenitor cells is their ability to rapidly respond to tissue damage<sup>1-3,5,47</sup>. To confirm that this capability is maintained *ex vivo*, we fed female flies Sodium dodecyl sulfate (SDS) mixed with solid fly food at a final concentration of 0.2% (v/w) for 18h. Following this treatment, the flies were fed 0.05% sucrose in aqueous solution on a cotton pad for an additional 4-6h prior to dissection, in order to flush the SDS from the gut. This protocol caused only mild initial tissue damage, and was advantageous as it did not result in the retention of high levels of SDS in explanted guts. However, by mixing the SDS-laced food with a blue food-safe dye, we found that some low amounts of SDS-laced food do persist in the lumen of intestines at the time of dissection. The transient exposure to SDS and the low amounts retained in the lumen resulted in gradual EC death and/or extrusion, allowing the live-imaging of damage response. When imaged, intestines from SDS-fed flies showed progenitor cells that become highly motile, similar to what was recently observed in similarly damaged intestines<sup>48</sup>. ISC proliferation events could also be detected (Figure 3C). However, ISC mitoses could generally be observed only in cases where tissue damage was extensive, as evidenced by the appearance of pyknotic or fragmented nuclei and the extrusion of multiple (> 3) contiguous ECs. As this tended to happen towards late time-points after dissection, only a few (1-2) mitotic events per imaged field could be observed with this damage protocol. In addition to ISC divisions, many progenitor cells could be observed growing in nuclear size while simultaneously losing GFP expression (Figure 3B,E-G and Videos 6-7), indicative of differentiation events towards the EC identity. Indeed, differentiating progenitor cells could be seen replacing dying enterocytes (Video 6).

We then tested whether these observations could be made in an *in vivo* condition. Before dissection, flies were fed either a control diet or SDS-laced food as described above. Flies dissected at later time-points (*i.e.* 24 and 48h after the initial SDS feeding) were kept on fresh food, thus allowing the intestine

to clear any trace of SDS and recover. This is different to the *ex vivo* condition, where a small amount of SDS is retained in the lumen and continues to damage the intestine during imaging. Although we found it impossible and impractical to perfectly match the luminal SDS content *in vivo* and *ex vivo*, the *in vivo* condition did confirm our *ex vivo* observations (Figure 3 – figure supplement 1). After SDS feeding, we observed several *esg*<sup>+</sup> cells with larger nuclei (Figure 3 – figure supplement 1A-B). At later time-points many differentiating cells with large nuclei and low GFP expression were also present, similar to what was observed *ex vivo*. Moreover, similarly to explanted midguts, proliferative cells could be found almost exclusively at 48h after the end of the SDS treatment (Figure 3 – figure supplement 1C).

A limitation of the SDS-feeding protocol described above is that midguts were damaged prior to imaging. Therefore, it cannot be excluded that the observed differentiation events were EBs that were poised to differentiate prior to SDS feeding, and then differentiated due to the damage stimulus. To confirm that, at the time of damage, pre-existing EBs were indeed capable of responding to tissue stress, we used a thin tungsten needle to create a small lesion in explanted intestines. The lesions perforated both visceral muscle and epithelial layers, but left the peritrophic matrix intact (Figure 3 – figure supplement 2A). Intestines were then enveloped in agarose and imaged within 20' of the time of damage. Similarly to the SDS damage protocol, we were able to record progenitor cells both dividing and differentiating (Figure 3 – figure supplement 2B,C and Video 8). Moreover, wounding stimulated the robust expression of the cytokine Unpaired 3 (*Upd3*), whose function in midgut damage response is well documented (Figure 3 – figure supplement 2D,E and Videos 9-10)<sup>3,49,50</sup>.

All in all, our observations suggest that both ISCs and EBs are quiescent in undamaged intestines. While previous studies did show varying rates of ISC proliferation in healthy midguts *in vivo*<sup>1-3,51,52</sup>, this may be attributed to cell death<sup>45</sup> as well as the passage of food through the intestinal lumen<sup>46</sup>, both of which do not occur in our midgut cultures until later time-points (*i.e.* after 48-72h). Moreover, several previous studies used lineage-tracing tools requiring a 37°C heat shock for their activation, a treatment known to



induce ISC proliferation<sup>4,52–55</sup>. Indeed, in the presence of tissue damage, progenitor cells could be robustly activated in explanted intestines, indicating that both ISCs and EBs are capable of responding to their environment after organ explant.

#### **Loss of *Notch* drives tumorigenesis *ex vivo***

A key pathway necessary for progenitor cell differentiation is the *Delta/Notch* signaling that occurs between ISCs and adjacent EBs<sup>1,2,56</sup>. The depletion of *Notch* (N) by RNA interference (*N<sup>RNAi</sup>*) in *esg*<sup>+</sup> cells has been shown to promote the formation of undifferentiated tumor-like masses *in vivo*<sup>1,2,49,56</sup>. Notably, tumor initiation by N-depleted ISCs requires proliferation induced by tissue stress<sup>49,57</sup>. Consistent with this, when we explanted midguts from flies expressing *N<sup>RNAi</sup>* in progenitor cells for 24h prior to dissection and cultured them for 48h, we did not observe tumorigenesis in the absence of tissue damage (Figure 3 – figure supplement 3A and Video 11). However, when guts were accidentally damaged during dissection (Figure 3 – figure supplement 3B, yellow ellipses), *esg*<sup>+</sup> cells started to proliferate (Figure 3 – figure supplement 3B, yellow squares, and Video 12). Notably, progenitor cells remained small and did not lose GFP expression (compare Figure 3B and Figure 3 – figure supplement 3B as well as Videos 5 and 12), suggesting a block of differentiation *ex vivo* in response to *Notch* knock-down.

#### **Intestinal progenitor proliferation can be genetically stimulated *ex vivo***

EGFR-Ras-Erk signaling is activated upon gut tissue damage, and this pathway is required for stem cell activation in the adult *Drosophila* intestine<sup>58–60</sup>. Previous experiments showed that expression of a constitutively active form of *Ras* (*Ras<sup>G12V</sup>*) strongly promotes stem cell proliferation in adult midguts<sup>60,61</sup>. As our culture protocol allows the expression of transgenes *ex vivo*, we induced *Ras<sup>G12V</sup>* in explanted midguts using the *esg-Gal4 Gal80<sup>TS</sup>* progenitor-specific driver gene combination (*esg<sup>TS</sup>*). When explanted midguts were shifted to the permissive temperature (29°C) at the start of imaging, progenitor cells, marked by GFP co-expressed with *Ras<sup>G12V</sup>*, started to rapidly proliferate (Figure 4B). About 20% of

progenitor cells tracked from the moment they expressed visible amounts of GFP till the end of the imaging session, were seen proliferating (Figure 4D). The progeny of observed mitoses were not counted for this analysis. However, since many cells were not trackable for the duration of the imaging session due to major tissue rearrangements, we may be underscoring the percentage of proliferative GFP<sup>+</sup> cells. As GFP<sup>+</sup> cells accumulated in the tissue, enterocytes were displaced and extruded from the epithelium (Figure 4B, yellow arrowhead, and Video 14). Interestingly, some GFP<sup>+</sup> progenitor cells did not proliferate, but their nuclei rapidly grew in size, which aligns with the previously reported role of EGFR signaling in promoting EB growth<sup>60,62</sup>. Moreover, these rapidly growing progenitors also lost GFP expression during the course of imaging, which suggests their differentiation towards the EC lineage.

The extended live-imaging that our protocol allows also permitted us to follow cells through multiple rounds of mitosis. Using manual 3-dimensional (3D) cell tracking, we reconstructed the lineages of 17 dividing cells that expressed *Ras*<sup>G12V</sup> (see Figure 5 and Video 16 for an example). As ISCs are the only cell type in the *Drosophila* intestine that normally divide multiple times<sup>1,2,63</sup>, the founding cells in these lineages were most likely ISCs. However, a recent work suggested that *Ras*<sup>G12V</sup> can push a small number of EBs to de-differentiate to an ISC state<sup>64</sup>. We directly measured the duration of progenitors' cell cycle in these lineages to be  $8 \pm 2.76$ h (Figure 4F). Interestingly, of 17 *Ras*<sup>G12V</sup>-expressing ISC lineages characterized, one had divisions where both daughter cells from the first recorded division were seen dividing further (Figure 4E). For simplicity, pairs of dividing daughter cells will be henceforth be referred to as "co-dividing siblings" (see Figure 6A-B and Video 17 for an example). These are most likely symmetric divisions that give rise to two new ISCs. However, since we did not track differentiation markers in our lineages, other possibilities cannot be excluded. For example, after being generated from an ISC division, enteroendocrine (EE) progenitors are also known to divide once to give rise to two mature EEs<sup>63</sup>. Moreover, we cannot exclude that cells that were not observed to divide during our imaging session would not divide again, given enough time.

284 Since *Ras*<sup>G12V</sup> stimulation results in multiple cellular changes, we also tested whether we could stimulate  
285 ISC proliferation more directly. For this we used the *esg*<sup>TS</sup> driver to co-express *string* (*stg*), a *Cdc25C*  
286 homolog, and *Cyclin E* (*CycE*) (Figure 4C and Video 13). String directly activates Cdk1 to promote mitosis,  
287 whereas CycE directly activates Cdk2 to promote DNA replication and S-phase progression. The  
288 combined expression of these two gene products is sufficient to strongly induce ISC proliferation<sup>65</sup>.  
289 Notably, Stg and CycE have also been shown to promote EB mitoses<sup>65</sup>, although much less strongly than  
290 in ISCs. The fraction of progenitor cells that divided in response to *stg* and *CycE* co-expression (~25%;  
291 Figure 4D) was not significantly different from that observed after forced expression of *Ras*<sup>G12V</sup>,  
292 suggesting that all receptive progenitors are activated in both cases. However, co-dividing siblings  
293 appeared in 6 of 12 ISC lineages that overexpressed *stg* and *CycE* (Figure 4E), a significantly higher  
294 frequency to the 1 of 17 observed after *Ras*<sup>G12V</sup> overexpression ( $p = 0.0106$ , Fisher's exact test). We  
295 detected no significant difference in cell cycle duration in progenitors' cell cycles driven by *stg* and *CycE*  
296 ( $9.4 \pm 4.6$ h) and cell cycles driven by *Ras*<sup>G12V</sup> ( $8 \pm 2.76$ h; Figure 4F), suggesting that their differing abilities  
297 to produce co-dividing sibling cells may reflect different effects on the differentiation process.

#### 298 **Co-dividing sibling cells actively move apart**

299 Combining all the lineages described above, we were able to identify 8 divisions that yielded co-dividing  
300 siblings (see Figure 6A-B and Video 16 for an example). For 7 of these, sibling cells divided within 2h of  
301 each other, while for one pair the interval was 5h. Based on this, we looked for divisions where one  
302 sibling cell was seen dividing further, while the other remained quiescent for the remainder of the  
303 experiment, which had to last at least 6h after the sister's mitotic event (*i.e.* the second division in the  
304 lineage). For simplicity, pairs of siblings with this behavior will be henceforth be referred to as "non-co-  
305 dividing siblings". These are most likely asymmetric divisions that give rise to an ISC/EB pair. However,  
306 since specific cell fate markers were not assayed in our experiments, this cannot be verified. Moreover,  
307 we cannot exclude that both cells would not eventually divide, given enough time. Regardless, the

308 behavior of these daughter pairs was indeed distinct from that of co-dividing siblings described above.

309 Following this definition, we classified 17 sibling pairs as non-co-dividing (see Figure 6D-F and Video 18

310 for an example), 9 from *Ras*<sup>G12V</sup>- and 8 from *stg* and *CycE*-expressing guts. Interestingly, for 8 of these 17

311 pairs, the non-dividing cells displayed increases in nuclear size over time, and also lost GFP expression,

312 which is indicative of differentiation towards the EC cell fate (Figure 6C,G-H). This behavior was not

313 observed for co-dividing siblings, where both cells increased their nuclear size before dividing further,

314 but maintained GFP expression (Figure 6A,E-F). Hence, future studies using our culture and imaging

315 techniques in conjunction with differentiation markers should be able to discern new details about ISC

316 differentiation.

317 It was previously reported that spindle orientation is indicative of whether an ISC mitosis is asymmetric

318 or symmetric, with symmetric divisions being planar relative to the visceral muscle layer, and

319 asymmetric divisions displacing one daughter cell apically, away from the visceral muscle<sup>22,56,66</sup>. As we

320 restricted the interval between subsequent imaging frames to 1h to reduce phototoxicity, we were not

321 able to measure spindle orientations. However, it has been proposed that the orientation of the mitotic

322 spindle results in daughter cells residing at different levels within the pseudostratified intestinal

323 epithelium, with new-born EBs being more apical<sup>56</sup>. We therefore selected mitotic events that occurred

324 in regions of epithelium that were flat with reference to the imaging plane (based on cell nuclei

325 positions). The 3D profile of sister cells after mitosis was then reconstructed and we measured the

326 angles between sister cells. Measured angles were found to be <15° in 29/33 cases for *Ras*<sup>G12V</sup>- and in

327 30/32 cases for *stg*+*CycE*-induced mitoses. Moreover, no significant differences in sister cell angles were

328 observed between co-dividing and non-co-dividing siblings (Figure 7A-C). These observations do not

329 support that view that apical displacement of daughter cells is associated with EB fate specification.

330 However, as we did not image the mitotic spindle during mitosis, it is possible that spindles were

oriented differently in divisions giving rise to the two sibling pair types, but that this difference in orientation was lost after cytokinesis.

A significant difference between co-dividing and non-co-dividing siblings was found, however, when we tracked newborn cells over time. Due to some cells having cell cycles lasting less than 8h, we only considered the first six 1h time-points following the appearance of a sister pair (defined as time-point 0). Measuring the distance between sister cells at each time interval, we found that cells in non-co-dividing pairs remained close to one another until the following mitotic event (Figure 7D, red line). Cells in co-dividing pairs, however, moved apart from one another (Figure 7D, green line). These behaviors could be observed even when considering unequal and co-dividing siblings in the same lineage (Figure 7E-F). If co-division and non-co-division are indeed indicative of symmetric and asymmetric division, respectively, this observation suggests that commitment to differentiation, as occurs after asymmetric divisions, requires that sister cells remain in contact for ~3-5 hours (Figure 7D,F, red line). This is in line with previous measurements of *Notch* activation dynamics in differentiating EBs<sup>21</sup>. Conversely, rapid separation of sister cells following a division may be necessary to generate a symmetric division that duplicates ISCs.

Differences in the motility of co-dividing and non-co-dividing siblings could explain these observed effects. We therefore measured cell motility as the distance in 3D space that a cell travelled between one time-point and the next. We found that the genotype used to induce proliferation did not have an effect on the cell motility of either sibling type (Figure 7 – figure supplement 1A). Likewise, no difference in cell motility was found when considering the effect of time on cell movement of non-co-dividing (Figure 7 – figure supplement 1B,C) or co-dividing (Figure 7 – figure supplement 1D) siblings. Therefore, we directly compared the motility of both pair types irrespective of genotype or time-point analyzed (Figure 7 – figure supplement 1E), but also found no significant difference. This indicates that cells of both pair types migrate within the epithelium at similar speeds. Since non-co-dividing siblings tend to

remain close to one another over time, their movement is most likely random. On the other hand, since the distance between co-dividing siblings increases over time, their movement is likely more directional, such that cells in a sibling pair move away from each other. It would therefore be expected that, when considering co-dividing pairs, the relative movement of one cell to its sister should be greater than that observed for non-co-dividing pairs. We therefore considered the motion of sister pairs, decomposing their movement in X- and Y-axis components and summed the resulting vectors, thus calculating the movement of a cell relative to its sister along the X- and Y-axis. As expected, the magnitudes of the reconstructed relative movements between co-dividing pairs was significantly greater than that for non-co-dividing pairs (Figure 7 – figure supplement 1F). This confirms that the movement of co-dividing cell pairs was directional, with the two cells moving away from one another right after division.

#### ***Ex vivo* culture of other adult *Drosophila* organs**

To test the feasibility of our culture setup to sustain other adult *Drosophila* organs, we first focused on the Malpighian (renal) tubules. Being physically connected to the intestine, we reasoned the two organs may share similar requirements for their survival *ex vivo*. A shared characteristic between Malpighian tubules and the adult midgut is the presence of a population of progenitor cells marked by *esg* expression<sup>67,68</sup>. Using the *esg*<sup>TS</sup> driver system, GFP expression could be induced in tubules cultured at 18°C for 24h and then shifted to the permissive temperature (29°C), indicating their long-term survival (Figure 8A-B). Moreover, we found that Malpighian tubules cultured for 3 days could still contract regularly (Video 19), albeit only if still attached to intestines.

A key component of our culture system that prolongs the viability of midguts is the co-culture with dissected abdomens and ovaries. On closer inspection, we found that adult hearts (the dorsal vessel), which lay along the abdominal cuticle, could be seen still beating regularly after up to 10 days in culture (Video 20). Similarly, the muscle sheet that envelopes the ovaries still contracted after 3 days in culture

(Video 21). We then took a closer look at ovaries by dissecting individual ovarioles for live-imaging. A distinctive characteristic of stage 1-8 follicles is their rotation within their follicle cell sheath, along their long axis<sup>69</sup>. In our *ex vivo* cultures, we routinely observed rotating stage 4 follicles that grew in size and started to elongate (Figure 8C-C' and Video 22), indicative of progression to stage 5<sup>69</sup>. Notably, this phenomenon continued for up to 48h, suggesting the long-term survival of follicles in our explants. Therefore, we believe our culture protocol could be applied to other adult *Drosophila* tissues and will be useful in investigating a wide range of biologically relevant phenomena.

## DISCUSSION

The adult *Drosophila* midgut has emerged as a powerful tool to understand the biology of epithelia and their resident stem cells. In recent years this system has been enriched by the development of advanced live-imaging approaches<sup>18–22</sup> that allow the observation of adult midguts for up to 16h. However, many biologically interesting processes, for instance regeneration, occur over longer time-spans, and so methods for extended culture and live-imaging should prove advantageous.

Several factors could cause the limited survival of midguts *ex vivo*. Firstly, currently available *Drosophila* culture media are based on larval hemolymph composition. We have shown here that minimal modifications to Schneider's medium are sufficient to reduce cell death *ex vivo* (Figure 2A). Midguts may also receive nutrients and signaling molecules from other organs such as ovaries and fat body, which are in close proximity to the intestine. Indeed, using fly extract as a culture medium and co-culturing intestines with ovaries and fly abdomens resulted in dramatic decreases in cell death (Figure 2A). Proper oxygenation is also a concern as it had been found to be essential for other *Drosophila* organ *ex vivo* cultures<sup>11</sup>. Indeed, trachea ramify throughout the fly's internal organs, and in the intestine they even reach through the visceral muscle to contact epithelial cells directly<sup>70</sup>. Therefore, we designed our culture setup to keep guts elevated and close to the surface of the culture medium at a liquid-air

401 interface (Figure 1), which we found to be important for proper tissue oxygenation. Moreover, the  
402 sample setup was designed to be efficient and simple to construct for ease of reproducibility, allowing  
403 up to 12 explanted midguts to be imaged in parallel in a single dish. Lastly, prolonged live-imaging  
404 sessions can be hampered by phototoxicity. This can be resolved by reducing the intensity of the  
405 excitation light and exposure times, albeit at the cost of reduced signal/noise ratios and frame rates.  
406 Controlling each of these factors has allowed us to culture healthy explanted midguts for up to 3 days *ex*  
407 *vivo* (Figure 2C and Video 2), and other organs for even longer periods.

408 Using our system, we observed that, while midguts maintain their ability to respond to tissue stress *ex*  
409 *vivo*, progenitor cells in undamaged intestines are quiescent. Previous estimates of mitotic rates based  
410 on immunostaining for the mitotic marker phospho-Ser 10-Histone 3 generally showed a wide range of  
411 baseline values, with numbers as low as 1-3 mitoses per midgut<sup>3</sup>. Nonetheless, even considering a low  
412 mitotic rate and using an estimate of mitosis duration<sup>21</sup> and ISCs numbers<sup>1,71-73</sup>, we expected to see  
413 several mitoses even in undamaged intestines (*e.g.* >5 for fields with 50 or more *esg*<sup>+</sup> cells). As ISC  
414 proliferation could be stimulated by tissue damage *ex vivo*, this suggests that, in homeostatic conditions,  
415 stem cells may only proliferate when the need to replace damaged or dying cells arises. Given the lack of  
416 cell death in undamaged midguts *ex vivo*, the previously reported proliferation-suppressive effect of  
417 enterocytes<sup>45,73</sup> may be responsible for the lack of observed mitotic events. Interestingly, we also did not  
418 observed differentiation events in undamaged intestines, which suggest that enteroblasts are a stable  
419 cell type, rather than being transient progenitors that are present only during periods of rapid ISC  
420 division, and are rapidly lost via differentiation or apoptosis<sup>51</sup>. Indeed, a previous analysis of the EB gene  
421 expression profile showed the existence of EB-specific genes, consistent with EBs being a distinct cell  
422 type<sup>74,75</sup>. As a consequence, the enteroblast pool may constitute a first line of response to tissue  
423 damage, that rapidly differentiate to generate new ECs, while buying time for stem cells to progress  
424 through the cell cycle.



425 Our culture system can also be used in combination with temperature-sensitive gene induction or  
426 knock-down tools, thus expanding its applications. When genetically stimulated by the expression of  
427 constitutively active *Ras*<sup>G12V</sup>, ISCs proliferated rapidly (Figure 4 and Video 14). Similarly, co-  
428 overexpression of *stg* and *CycE* also resulted in ISC proliferation. These are strong genetic manipulations  
429 known to promote ISC proliferation. Glycine 12 mutations in KRAS, which result in the constitutive  
430 activation of the small GTPase, are among the most frequent mutations in colorectal and other  
431 cancers<sup>76</sup>. In the adult *Drosophila* intestine, this same mutation (G12V) has been shown to drive ISC  
432 proliferation<sup>60,61</sup>, and EB growth and endoreplication<sup>62</sup>. Moreover, a recent study suggested that a small  
433 subset of EBs could also be induced to proliferate by *Ras*<sup>G12V64</sup>. Co-overexpression of *stg* and *CycE* can  
434 also promote ISC proliferation by directly stimulating cell cycle progression<sup>65</sup>. Similarly to *Ras*<sup>G12V</sup>, this  
435 genetic stimulation could also drive EB proliferation, albeit not as strongly as in ISC. It's reasonable to  
436 assume that the EBs responsive to either *Ras*<sup>G12V</sup> or *stg* and *CycE* co-expression may be immature and  
437 still close to a stem cell state. When reconstructing cell lineages induced by these genetic manipulations,  
438 we observed divisions that gave rise to daughter cells with two distinct behaviors: 1) "co-dividing" pairs  
439 in which both daughter cells divided again, like the progeny of symmetric divisions; and 2) "non-co-  
440 dividing" pairs in which only one daughter cell divided while the other did not for the remainder of the  
441 imaging session (>6h), as would be the case for the progeny of asymmetric divisions. By analyzing the  
442 reconstructed lineages, we found that upon *Ras*<sup>G12V</sup> stimulation most lineages did not present co-  
443 dividing siblings. Interestingly, if co-dividing siblings were the result of symmetric divisions, this would be  
444 in accordance to the previously described prevalence of asymmetric division events in normal  
445 intestines<sup>52,72</sup>. This could suggest that the EGFR-Ras-Erk pathway may have a role in differentiation.  
446 Indeed, several progenitor cells, when stimulated by *Ras*<sup>G12V</sup>, did not divide, but rapidly grew in nuclear  
447 size and lost *esg* expression, which is indicative of EB to EC differentiation and a similar phenotype to

what previously reported<sup>62</sup>. Alternatively, Stg and CycE overexpression may suppress differentiation, resulting in the increased number of symmetric-like divisions we observed (Figure 4E).

One major difference that we did observe between co-dividing and non-co-dividing siblings was in the behavior of sister cells. Non-co-dividing siblings remained close to one another for several hours after mitosis. This is significant as it is known that cell-cell contacts between progenitor cells are required for promoting differentiation<sup>1,2</sup>. Indeed, interactions between Notch on the surface of the EB and Delta expressed on the ISC surface is a strong promoter of EB to EC differentiation<sup>1,2,56</sup>. It was previously shown that EB differentiation via N activation requires several hours to resolve<sup>21</sup>. This time frame matches our observations, which show non-co-dividing sister pairs remaining in contact for at least ~3-5 hours after division. Adherens junctions may be affecting these cell contacts as strong levels of shotgun (e-cadherin) and armadillo ( $\beta$ -catenin) are found in between ISC and EB pairs<sup>71</sup>. As EGFR signaling is known to impact adherens junctions remodeling<sup>58,77,78</sup>, this could help explain the prevalence of non-co-dividing siblings in cell lineages stimulated by *Ras*<sup>G12V</sup> expression. Co-dividing pairs had the opposite behavior, and moved apart right after division. If co-dividing siblings were the result of symmetric division expanding the ISC pool, this would result in the dispersion of stem cells through the midgut. As symmetric divisions are known to occur during adaptive growth of the intestine, especially in the days after eclosion, this behavior could help explain how ISCs space themselves uniformly in the epithelium<sup>72,79</sup>.

Despite these successful applications, the system we developed still has limitations. The optimized dissection procedure limits midgut damage, but does not completely eliminate the risk. The agarose pads, albeit thin, can interfere with high powered objectives with short working distances (*e.g.* 40X and above). Using thinner agarose pads could help to reduce the required working distance, but may result in hypoxia. This in turn could be solved by increasing the oxygen concentration using microscope incubation chambers equipped with an atmosphere control unit. Midgut survival *ex vivo* also seems to

472 be limited by the growth of enteric bacteria, especially since, once dissected, midguts cannot properly  
473 move food through the intestine and defecate. Indeed, we observed that the visceral muscle, which is  
474 not in direct contact with luminal contents, could survive and contract regularly for up to a week in  
475 optimal conditions, despite the death of the adjacent epithelium. Generating axenic flies may help to  
476 further extend the survival of the midgut epithelium *ex vivo*. Newer, gentler imaging technologies such  
477 as light-sheet microscopy could also improve survival during live-imaging sessions by reducing  
478 phototoxicity. It's also possible that different organs may have specific requirements in terms of media  
479 composition and additives, in which case tailoring culture media to a specific organ may be beneficial.  
480 Indeed, even the same organ can have different requirements in male and female flies<sup>79-81</sup>. Lastly, to  
481 limit mechanical damage to the intestines and to more easily image them, we used the calcium blocker  
482 isradipine to inhibit visceral muscle peristalsis. The lack of peristaltic contraction may have negative  
483 effect on midgut biology, aside from the retention of food and proliferating bacteria in the lumen.  
484 Indeed, it was previously reported that ISCs are sensitive to mechanical stimuli<sup>20</sup>. If food passage itself  
485 can stimulate ISC proliferation, its inhibition could partially help to explain the lack of mitosis in healthy  
486 midguts *ex vivo*.

487 Nonetheless, the increased survival *ex vivo* our protocol allows is significant and we believe it can enable  
488 experiments that will lead to a better understanding of the mechanisms that mediate epithelial  
489 homeostasis, such as the regulation of asymmetric and symmetric ISC division events. Our protocol may  
490 also provide a platform to dissect inter-organ interactions, given the positive effect that co-culture with  
491 ovaries and fat bodies had on midgut survival (Figure 2A). Moreover, Malpighian tubules, hearts, and  
492 ovaries did show increased survival when cultured with our protocol (Figure 8 and Videos 17-20). Finally,  
493 we believe that the possibility to visualize the effects of gene induction or silencing in real-time using  
494 fluorescent markers will be very useful for dissecting the roles of specific signaling pathway components  
495 and in modeling human disease.

496 **MATERIALS AND METHODS**

497 ***Drosophila* stocks**

498 *w*<sup>1118</sup> (Bloomington Drosophila Stock Center 3605)

499 *esg-Gal4 tubGal80ts UAS-GFP / CyO; UAS-flp Act>CD2>Gal4 / TM6B* (PMID: 19563763)

500 *esg-Gal4 Tub-Gal80<sup>TS</sup> UAS-nlsGFP / CyO*

501 *mex-Gal4 Tub-Gal80<sup>TS</sup> UAS-GFP / CyO*

502 *esg-Gal4 UAS-GFP*

503 *esg-Gal4 Tub-Gal80<sup>TS</sup> UAS-nlsGFP / CyO; His2Av-mRFP / TM6B*

504 *His2Av-mRFP* (Bloomington Drosophila Stock Center 23650)

505 *UAS-N<sup>RNAi</sup> / TM6B* (PMID: 26237646)

506 *UAS-Ras<sup>G12V</sup> / CyO* (PMID: 21167805)

507 *UAS-stg, UAS-CycE* (PMID: 24975577)

508 *PCNA-GFP* (Stefano Di Talia, Duke University Medical Center, USA)

509 *His2Av-mRFP; PCNA-GFP*

510 **Fly rearing**

511 Flies were raised on standard cornmeal and molasses fly food. Prior to dissection, flies were flipped to  
512 fresh vials without live yeast daily for 3 days at 18°C to reduce the load of commensal bacteria. On the  
513 morning of the dissection, flies were fed a sucrose 0.05% aqueous solution on a cotton pad at room  
514 temperature (25°C) for 4-6h to clear most luminal contents. This also helped to reduce accumulation of  
515 food in the posterior section of the gut, which could lead to the mechanical stress of the epithelium. For

516 SDS feeding experiments, flies were fed overnight either standard food or food mixed with SDS to a final  
517 concentration of 0.2% v/w. Both foods were also mixed with a blue food-safe dye to control for feeding.  
518 The following morning, flies were fed a sucrose 0.05% aqueous solution on a cotton pad to clear most of  
519 the luminal SDS.

520 **Modified Schneider's medium for adult *Drosophila* tissues.**

521 Schneider's medium (Genesee Scientific, 25-515) was modified by adding the following reagents to the  
522 stated final concentrations: 1mM trisodium citrate dihydrate (ThermoFisher Scientific, BP327), 91.2mM  
523 sodium chloride (Sigma-Aldrich, S9888), 55.8mM D-trehalose anhydrous (Sigma-Aldrich, T0167), 10mM  
524 glutamine (Gibco, 25030), and 2mM N-acetyl cysteine (Sigma-Aldrich, A7250) (Table 1). Glutamine needs  
525 to be added only if the batch of Schneider's medium used is glutamine-free. Medium was then filtered  
526 using 0.22µm syringe filters (VWR, 28145) and stored at 4°C. See Supplementary File 1 for recipe. This  
527 medium was used without additives during dissection, agarose gel stock preparation, and as a base for  
528 fly extract.

529 For fly extract, well-fed female flies were anesthetized on ice. Using mortar and pestle, flies were  
530 homogenized on ice in the presence of 10% per mg of flies of modified Schneider's medium (as  
531 described above) with bovine serum albumin (BSA) added to 1%. The homogenate was centrifuged at  
532 0.6G and 4°C for 10'. Supernatant was saved and fly carcasses discarded. The centrifugation step was  
533 repeated 3 times until all solid fly residues were eliminated. Extract was heat inactivated by heating at  
534 60°C for 5', then centrifuged at 0.6G and 4°C for 10'. Supernatant was saved and filtered using 0.22µm  
535 syringe filters. Extract was aliquoted and stored at -20°C before use.

536 For live-imaging, 100% fly extract prepared in modified Schneider's medium was used as a base for the  
537 complete culture medium. Fly extract was slowly thawed at 4°C, then 10% fetal calf serum (Gibco,  
538 26140079), 1:100 Antibiotic-Antimycotic (ThermoFisher Scientific, 152400062), 100µg/ml Ampicillin

539 (Fisher Scientific, AC611770250), and 25µg/ml Chloramphenicol (Fischer Scientific, BP904-100) were  
540 added. To suppress peristaltic movements, 10µg/ml isradipine (SigmaAldrich, I6658) was added to the  
541 complete medium immediately before imaging.

542

Component	Schneider's medium	Modified Schneider's medium
<b>Amino Acids</b>	<b>Concentration (mM)</b>	<b>Concentration (mM)</b>
Glycine	3.3	3.3
L-Arginine	2.3	2.3
L-Aspartic acid	3.0	3.0
L-Cysteine	0.5	0.5
L-Cystine	0.4	0.4
L-Glutamic Acid	5.4	5.4
L-Glutamine	12.3	12.3
L-Histidine	2.6	2.6
L-Isoleucine	1.1	1.1
L-Leucine	1.1	1.1
L-Lysine hydrochloride	9.0	9.0
L-Methionine	5.4	5.4
L-Phenylalanine	0.9	0.9
L-Proline	14.8	14.8
L-Serine	2.4	2.4
L-Threonine	2.9	2.9
L-Tryptophan	0.5	0.5
L-Tyrosine	2.8	2.8
L-Valine	2.6	2.6
beta-Alanine	5.6	5.6
<b>Inorganic Salts</b>		
Calcium Chloride (CaCl <sub>2</sub> ) (anhyd.)	5.4	5.4
MgCl <sub>2</sub> Hexahydrate	0.0	0.0
Magnesium Sulfate (MgSO <sub>4</sub> ) (anhyd.)	15.1	15.1
Potassium Chloride (KCl)	21.3	21.3
Potassium Phosphate monobasic	3.3	3.3
Sodium Bicarbonate (NaHCO <sub>3</sub> )	4.8	4.8
Sodium Chloride (NaCl)	36.2	91.2
Sodium Phosphate dibasic (Na <sub>2</sub> HPO <sub>4</sub> )	4.9	4.9
<b>Other Components</b>		
N-Acetyl Cysteine	0.0	2.0
Trisodium Citrate Dihydrate	0.0	1.0
Alpha-Ketoglutaric acid	1.4	1.4
D-Glucose (Dextrose)	11.1	11.1
Fumaric acid	0.9	0.9
Malic acid	0.7	0.7
Succinic acid	0.8	0.8
Trehalose	5.8	55.8
Yeastolate (g/l)	2000.0	2000.0

**Table 1: Modified Schneider's medium formulation.** Components whose concentration was modified are highlighted in yellow.

543

544

### Sample preparation for long-term culture and live imaging

1. Prior to dissection, a 35mm dish with lockable lid (ibidi®, µ-Dish 35 mm low, 80136) is prepared by first placing a thin wet paper tissue around its inner rim to reduce evaporation during long imaging sessions (Figure 1O, left panel);
2. Agarose pads are then cast by spreading 2µl of low gelling temperature agarose (Sigma Aldrich, A9414), heated to 70°C, over four 4mm areas in the observation region of the dish. For each dish, 4 pads can be easily cast (Figure 1O, left panel). The agarose solution is prepared from powder as a 1% stock in modified Schneider's medium without additives and stored at 4°C in 200µl aliquots. Aliquots can be melted and re-gelled several times, provided evaporation is not excessive;
3. Dishes are then stored at room temperature while midguts are isolated by dissection;
4. A small amount of medium is then added to the top of each agarose pad to facilitate the transfer of midguts. These are transferred very carefully, by holding them in a drop of liquid in between the grasping ends of a forceps. The drop is then touched to the top of an agarose pad, gently depositing the midgut trapped in it. Care must be exercised to ensure that the midgut rests entirely within the drop of liquid, without touching the dry surfaces of the forceps, to which it may stick. Each agarose pad can house up to 3 guts;
5. Once all midguts have been transferred, liquid from the top of the agarose pads is removed as much as possible using forceps, while leaving a small amount to avoid desiccation of the intestines. Midguts are then gently repositioned for proper imaging, if required;
6. Guts are then covered with a thin layer of low gelling temperature agarose 0.5% cooled to 37°C (Figure 1O, middle panel). The layer must be just enough to cover the midguts' surface (~1µl per pad);



7. The sample is incubated for 5 min at room temperature before the agarose structures are connected between them and to the sides of the observation area by creating agarose bridges with 0.5% low gelling agarose (Figure 1O, middle panel). This increases the stability of the overall sample, facilitating its transport in case the sample has to be prepared at some distance from the microscope that will be used to image it. If required, agarose domes can also be strengthened with an additional thin layer of agarose;
8. After 10 min, the agarose will have solidified and 120µl of complete culture medium can be carefully added to the sample (Figure 1O, right panel). The small volume is enough so that all midguts will receive nutrients throughout the culture duration, while ensuring that the uppermost surface of the agarose structures is not submerged by liquid, creating a liquid-air interface;
9. Finally, ovaries and fly abdomens that were dissected along with the midguts are added to the culture, free-floating in between the agarose pads. The sample will thereby be ready for imaging;

#### **Optimized dissection to avoid damaging of midguts.**

1. To reduce the risk of contamination of the culture by bacteria residing on the animal exterior, CO<sub>2</sub> anesthetized flies are surface sterilized by submerging them in 70% ethanol for 2 min and then in 50% bleach for 1 min. Most flies survive this treatment;
2. Flies are then washed and stored in 1X PBS modified as they are dissected one by one in modified Schneider's medium without additives. Since this step is fast (< 2 min), using complete medium based on fly extract is not required;
3. Using micro-scissors the head is removed with a clean cut, thus ensuring that the crop and proventriculus still reside in the fly thorax (Figure 1B,C; Video 1);
4. The cuticle around the anus is pulled, exposing the hindgut (Figure 1D);

5. Holding the fly gently with forceps around the thorax-abdomen junction, the soft ventral abdominal cuticle is ripped using another forceps, pulling it along the length of the fly towards the anus, thus exposing the midgut (Figure 1E,F; Video 1);
6. The abdomen is then gently separated from the thorax (Fig . 1G; Video 1);
7. The crop is gently pinched and pulled out of the thorax, thus freeing the anterior midgut along with it (Figure 1H,K yellow arrowhead; Video 1);
8. The midgut is gently freed from the abdominal cuticle (Figure 1J; Video 1). Care has to be exercised at this step as many trachea filaments connect the midgut to ovaries and abdominal walls. Freeing the midgut from ovaries and the abdominal cuticle is important for ease of handling and imaging and for proper oxygenation. Indeed, if these structures are kept attached to the intestine, transferring the explanted organ to agarose pads is harder and carries the risk of the midgut being covered by ovaries and the cuticle, thus limiting imaging access and creating a barrier between the midgut and the air-liquid interface;
9. Crop and malpighian tubules are cut away using micro-scissors, and the hindgut is similarly removed just below its connection to the midgut (Figure 1K-M; Video 1). This step is necessary as both Malpighian tubules and the ampulla connected to the hindgut are quite sticky and make transferring the guts to the imaging dish difficult. If desired, however, Malpighian tubules can be transferred to agarose pads for imaging, either detached or still connected to midguts;
10. Once dissected, a midgut can then be transferred to a well containing modified Schneider's medium with 10µg/ml isradipine. Ovaries and the fly abdomen are transferred to this well too;
11. Once all midguts have been dissected, they can be carefully transferred to the agarose pads for sample preparation. To avoid damage during transfer, it is recommended that midguts be moved by keeping them in a small drop of liquid in between the prongs of a forceps. Ovaries and

fly abdomens to be co-cultured with the intestines are transferred to the space between the agarose pads, free-floating in the culture medium;

12. For localized damage experiments, midguts were poked in their posterior section using an electrolytically sharpened tungsten needle once transferred to the agarose pads. To keep guts still during the procedure, the hidgut section can be clamped with forceps held in the non-dominant hand. For this, a longer hidgut section can be preserved (see point 9). It is imperative to avoid perforating the peritrophic matrix, thus preventing the contamination of the culture from commensal bacteria. For this, guts are not perforated perpendicularly to the epithelium, but at a ~45° angle. Alternatively, guts can be carefully scratched repeatedly in the same spot to produce a tear;

#### **Long-term live-imaging of explanted adult *Drosophila* midguts**

For imaging of midgut, hearts, and Malpighian tubules we used an inverted widefield Nikon Ti Eclipse microscope equipped with an incubation chamber (Okolab) for moisture and temperature control, a CoolSnap HQ2 camera (Photometrics), a SOLA LED light engine (Lumencore), and a Prior motorized stage. To limit phototoxicity, albeit at the cost of reduced signal/noise ratio, we used a 4x neutral density filter, limited light intensity to 5%, and limited exposure times to 100-150ms and 200-300ms for GFP and RFP signals, respectively. Follicles were imaged using a Leica SP8 confocal microscope equipped with a white laser light source and an incubation chamber (Okolab). To limit dwell time, samples were imaged at a frequency of 700Hz. Intestines could also be successfully imaged with the same setup. For both widefield and confocal setups, videos were captured at room temperature (25°C) or at 29°C for temperature-sensitive gene induction experiments using a 20X air objective (APO 20X NA 0.75 WD 1). Multipoint acquisition was used to image the R4-5 posterior midgut section of 12 intestines during each imaging section. For each midgut, a 45µm Z-stack was captured using a 3µm Z-step. Focus was manually checked and corrected during the course of the imaging session with the Nikon Ti Eclipse, or using a

contrast-based autofocus routine for the Leica SP8. Frame rate was typically one full multi-channel Z-stack/midgut/hour. For the imaging of Malpighian tubules and ovaries contractions and beating hearts, the frame rate was 1 slice every 0.08ms instead.

#### **NucGreen analysis**

For cell survival experiments, guts from W<sup>1118</sup> flies were cultured in media containing NucGreen (ThermoFisher Scientific, R37109) diluted 1:20. Midguts were imaged once a day for 3 days, using a 10X air objective (Plan Fluor 10X NA 0.3 WD 16) to capture a stitched z-stack of the whole organ with z-steps of 20µm. Images were normalized to their median pixel value to account for changes in background, then midgut areas were manually selected from maximum intensity projections. The NucGreen signal was computed as the sum of pixel values in the selected areas, normalized to the first time-point in the series.

#### **GFP level quantification**

Midguts were explanted from 5-15 days old flies reared at 18°C and cultured at 29°C for 24h. Midguts were then carefully removed from the culture setup and fixed in para-formaldehyde 6% in PBS for 30 minutes at room temperature. Similarly, *in vivo* control flies were shifted to 29°C for 24h, then dissected and their midguts fixed. Fixed intestines were stained for DAPI 0.1mg/ml (Sigma-Aldrich, 10236276001) in PBS with 0.1% Triton-X100, then mounted with VECTASHIELD® antifade mounting medium (Vector Laboratories, H-1000-10). The posterior region of the intestines was imaged and the GFP and DAPI signals were thresholded using Otsu's method<sup>82</sup>. Regions of overlap between the two thresholded channels were used as a mask to calculate the mean GFP expression of each cell of interest in the imaged field. For each intestine, the values of each measured cell were averaged to express a mean fluorescence for the whole intestine.

For GFP induction tests, malpighian tubules were detached from midguts using micro-scissors and cultured in sandwiched agarose structures as described above. Tubules were cultured at 18°C for 24h then at 29°C. Images were captured daily. Individual GFP<sup>+</sup> cells from 48h images were identified in previous time-points and their GFP intensity measured.

#### **Cell tracking and analysis.**

Image analysis was performed using either ImageJ or Python (v3.7.10). Using a custom Python script (Source code 1), each time-lapse movie was divided at the first time point into overlapping regions of interest that were then used for automatic local registration. This helps account for local movements and deformations of the intestinal epithelium which complicate the following image analysis step. Registration was based on cross-correlation of a region of interest with the next frame of the time-series. Individual ISC and their progeny were then manually tracked using a custom ImageJ macro (Source code 2), selecting each cell by drawing their outline at their most in-focus z slice. By identifying all cells between successive time-points, we avoided lineage assignment errors even with long time-intervals between frames.

Cells were then analyzed as follows:

- Lineages were reconstructed with a custom Python script (Source code 3) using the cell positions in the imaged field across time annotated during manual tracking. When the former approach failed due to too complex rearrangements of cells within a lineage, lineages were manually annotated instead;
- Nuclear size was measured during manual tracking from the most in-focus z-slice using an upscaled image so as to achieve sub-pixel precision;
- Mean nuclear GFP intensity was measured during manual tracking and adjusted to the median value in a 50µm window around the cell of interest to account for changes in local background;

- Cell cycle duration was measured as the number of frames (each representing a 1h interval) from the appearance of a cell resulting from a mitotic event and its subsequent division;
- Cell motility was defined as the distance between the positions of a cell in two subsequent frames. We used the center nuclei to mark cells' positions. Since *esg*<sup>+</sup> cells have a high nuclear/cytoplasm ration, measuring internuclear distance is a good approximation for quantifying cell motility. A few errors during image registration resulted in improper measurements, which were then discarded. For this, outlier values were first identified using the interquartile range method, then confirmed on the registered movie file;
- For analysis of the angle between sister cells, the z-profile along the axis connecting the center of the two cells was reconstructed Python. Only cells in flat sections of epithelium in reference to the imaging plane (based on enterocytes' nuclei positions) were considered. The pixel values of the stack along a line connecting the two cells were used to reconstruct the 3D profile. Once all profiles were reconstructed, the angle between the 3D centers of the sister cells was manually computed in reference to the imaging plane. Measurements were repeated three times and averaged.

## ACKNOWLEDGEMENTS

This work was supported by the Huntsman Cancer Foundation, and National Institutes of Health Grants R01 GM124434 and R35 140900 (to B.A.E.) and P30 CA042014. We thank the Bloomington Drosophila Stock Center for fly stocks. We thank the University of Utah Cell Imaging Core for its instruments and assistance.

## COMPETING INTERESTS

The authors declare no competing interests.

## FIGURE LEGENDS

**Figure 1: Sample preparation for live-imaging.** (A-N) Minimal handling dissection used to gently explant adult *Drosophila* midguts, limiting the risk of damaging the intestines. See also Video 1. (O) Culture chamber setup (left) and mounting of explanted midguts (middle and bottom diagram) to produce an air-liquid interface culture (right). See methods section and Video 1 for in-depth description.

**Figure 2: A custom culture medium sustains the midgut *ex vivo*.** (A) Incorporation of the cell-impermeable dye NucGreen shows the levels of midgut cell death *ex vivo* in midguts cultured in: standard Schneider's medium (SM), modified Schneider's medium (MSM), MSM with 10% added fetal calf serum (FCS), MSM including co-culture with fat bodies and ovaries (FbO), culture in fly extract prepared in MSM (FeMSM), and the combination of all these conditions (Complete). Error bars represent the standard error of the mean. (B) Explanted midguts maintain their shape and tissue integrity for 3 days in culture. However, commensal bacteria keep growing in the lumen, especially in the posterior section where this can be seen as a darkening of the lumen (white arrows). Scale bar is 100µm. (C) Maximum intensity projection of intestine expressing a lineage-tracing system under *esg*<sup>TS</sup> driver and imaged for 72h at 29°C. The fly of origin was incubated at 29°C for 24h prior to dissection. The intestine was undamaged during the course of imaging and did not show proliferation events. Scale bar is 5µm. See also Video 2. (D-E) Temperature-sensitive gene induction *ex vivo* is possible in both progenitor cells (D) and enterocytes (E). GFP levels expressed after 24h of gene induction are comparable between *in vivo* and *ex vivo* intestines. Explanted intestines were shifted to 29°C immediately after sample preparation. *In vivo* controls were shifted simultaneously. Images are representative maximum intensity projections of posterior midguts. Scale bar is 50µm. Each dot in the graphs represents the average GFP expression level in the posterior section of an intestine (T test). (ns, not significant)

**Figure 3: Midguts respond to damage *ex vivo*.** (A) Healthy gut fed a control diet showing no sign of tissue damage. Images are maximum intensity projections. See also Video 4. Scale bar is 20µm. (B) Gut

731 from fly fed SDS 0.2% overnight showing progressive tissue repair *ex vivo* mediated by progenitor cells  
 732 proliferation and differentiation. As cells differentiate, nlsGFP expression is gradually lost. Area  
 733 delimited by the yellow rectangle is enlarged in (B'). Images are maximum intensity projections. See also  
 734 Video 5. Scale bar is 20µm. (B') Enlargement of panel (B) showing an *esg*<sup>+</sup> cell (white outline)  
 735 differentiating and replacing dying enterocytes (yellow circles). As the cell differentiates, nlsGFP  
 736 expression is lost and its nucleus grows larger. Images are maximum intensity projections. See also  
 737 Video 6. Scale bar is 10µm. (C) Example of stem cell dividing upon tissue damage initiated by SDS  
 738 feeding. Cell is marked by the expression of nlsGFP (yellow arrowhead). Note that in the 30h time-point  
 739 the cell is in mitosis and so the nlsGFP signal is mostly lost due to nuclear envelope breakdown. After  
 740 mitosis, the nuclear envelope is reformed and GFP re-accumulates in the nucleus of the daughter cells.  
 741 Images are single z-slices. Scale bar is 5µm. (D) Plots of nuclear area (red) and mean nuclear GFP  
 742 intensity (green) from single progenitor cells from healthy guts. Note that both nuclear size and GFP  
 743 signal, despite a small gradual dip caused by photobleaching, are stable for the duration of the imaging  
 744 session. See also Video 7, left column. (E) Plots of nuclear area (red) and mean nuclear GFP intensity  
 745 (green) in single progenitor cells from SDS-damaged guts. Note that nuclear size increases, while GFP  
 746 signals dims over time, suggesting EB to EC differentiation. See also Video 7, right column. (F)  
 747 Quantification of nuclear area of *esg*<sup>+</sup> cells in control (green) and SDS-damaged (red) intestines cultured  
 748 *ex vivo*. Each cell was measured at imaging start (i.e. 0h) and 48h later. In control guts, *esg*<sup>+</sup> cells remain  
 749 quiescent and have no change in nuclear size. Due to the SDS treatment, several progenitor cells have a  
 750 large nucleus already at the time of dissection. Furthermore, most progenitor cells' nuclear area  
 751 significantly increases during the course of imaging (Two-way Anova and Šídák's multiple comparisons  
 752 test). (G) Ratio of nuclear GFP intensity for individual *esg*<sup>+</sup> cells from control or SDS-damaged intestines  
 753 cultured *ex vivo*. While cells in control intestines do not lose GFP expression (except for a minor loss due  
 754 to photobleaching), several cells in the SDS-treated intestines show a significant loss of GFP intensity,



suggesting their differentiation and change of cell identity (T test). (ns, not significant, \*,  $p < 0.05$ ; \*\*\*\*,  $p < 0.0001$ )

**Figure 4: Genetic induction of intestinal stem cell proliferation.** (A) Live-imaging of a normal intestine expressing nlsGFP in progenitor cells via *esg<sup>TS</sup>* driver. Intestines were shifted to 29°C at the start of imaging. Note the gradual accumulation of GFP signal showing variability between cells in terms of both time and intensity. Images are maximum intensity projections. See also Video 13. Scale bar is 20µm. (B) Live-imaging of an intestine expressing nlsGFP and *Ras<sup>G12V</sup>* in progenitor cells via *esg<sup>TS</sup>* driver. Intestines were shifted to 29°C at the start of imaging. GFP<sup>+</sup> cells can be seen rapidly dividing and displacing mature enterocytes (yellow arrowhead). Images are maximum intensity projections. See also Video 14. Scale bar is 20µm. (C) Live-imaging of an intestine expressing nlsGFP, *stg*, and *CycE* in progenitor cells via *esg<sup>TS</sup>* driver. Intestines were shifted to 29°C at the start of imaging. GFP<sup>+</sup> cells can be seen rapidly dividing. Images are maximum intensity projections. See also Video 15. Scale bar is 20µm. (D) Quantification of observed proliferating and non-proliferating *esg<sup>+</sup>* progenitor cells in control and intestines expressing *Ras<sup>G12V</sup>* or *stg* and *CycE*. Only cells observed from the moment they expressed visible levels of GFP to the end of the imaging session are included. The progeny of observed mitoses were not counted for this analysis. (E) Frequency of stem cell lineages with divisions giving rise to two proliferative cells (green), compared between intestines expressing either *Ras<sup>G12V</sup>* or *stg* and *CycE* (Fisher's exact test). (F) Quantification of cell cycle durations of progenitor cells expressing either *Ras<sup>G12V</sup>* or *stg* and *CycE*, and nlsGFP. No significant difference was found between the two genotypes (Mann-Whitney test). (ns, not significant; \*,  $p < 0.05$ )

**Figure 5: Example of a reconstructed ISC lineage.** (A) Time-lapse of a single *Ras<sup>G12V</sup>*-expressing ISC undergoing multiple rounds of mitoses. The nlsGFP channel is shown. Cells belonging to the lineage are marked by yellow arrowheads. (B) Lineage diagram. Cells visible at the last time-point shown are marked

778 in magenta. Images are maximum intensity projections of z-slices encompassing the cells in the lineage.  
 779 See also Video 16. Scale bar is 5µm.

780 **Figure 6: Examples of asymmetric and symmetric divisions.** (A) nlsGFP channel showing a stem cell  
 781 undergoing division upon expression of *stg* and *CycE* via *esg<sup>TS</sup>* driver and giving rise to co-dividing  
 782 siblings. The resulting daughter cells (green arrowheads) can be seen further dividing at the 41h and 42h  
 783 time-points. A white circle denotes the outline of the starting cell at the initial time-points, when signal  
 784 was weakest. Images are maximum intensity projections of z-slices encompassing the cells in the  
 785 lineage. See also Video 17. Scale bar is 5µm. (B) Lineage diagram for cell in A. Green branch denotes co-  
 786 dividing siblings. Cell present at the end of the imaging session are marked by magenta dots. (C) nlsGFP  
 787 channel showing a stem cell undergoing division upon expression of *Ras<sup>G12V</sup>* via *esg<sup>TS</sup>* driver giving rise to  
 788 non-co-dividing siblings. Of the resulting daughter cells (red arrowheads), only one can be seen dividing  
 789 further. The non-dividing cell is observed for at least 6h following the division of its sister cell. Images  
 790 are maximum intensity projections of z-slices encompassing the cells in the lineage. See also Video 18.  
 791 Scale bar is 5µm. (D) Lineage diagram for cell in C. Red branch denotes non-co-dividing siblings. Cell  
 792 present at the end of the imaging session are marked by magenta dots. (E-H) Plots of nuclear area (E, G)  
 793 and nuclear GFP mean intensity (F, H) for the lineage in A (E-F) and C (G-H). Dotted lines connect mitotic  
 794 cells to their progeny. Green and red lines denote co-dividing and non-co-dividing siblings, respectively.  
 795 The GFP channel was used for quantification.

796 **Figure 7: Analysis of non-co-dividing and co-dividing siblings in the *Drosophila* midgut.** (A) Angle  
 797 between daughter cells after mitosis as referenced to the imaging plane. No difference was found  
 798 between the two types of daughter pairs (Mann-Whitney). (B) XY (top panel) and Z (bottom panels)  
 799 nlsGFP profiles of the division event from Figure 6A,B giving rise to co-dividing siblings. Cell proliferation  
 800 was stimulated by *esg<sup>TS</sup>*-driven expression of *stg* and *CycE*. Scale bar is 5µm. (C) XY (top panel) and Z  
 801 (bottom panels) nlsGFP profiles of the division event from Figure 6C,D giving rise to non-co-dividing

siblings. Cell proliferation was stimulated by *esg<sup>TS</sup>*-driven expression of *Ras<sup>G12V</sup>*. Scale bar is 5µm. (D) Internuclear distance between daughter cells in the first 5h after mitosis. Time point 0h denotes the first at which the two daughter cells are visible. Error bars represent standard deviation (Two-way Anova and Šídák's multiple comparisons test). (E) Example of lineage characterized by both non-co-dividing (red) and co-dividing siblings (green). Cell proliferation was stimulated by *esg<sup>TS</sup>*-driven expression of *stg* and *CycE*. (F) Internuclear distance between the non-co-dividing and co-dividing sister cells from the lineage in E. Time point 0h denotes the first at which the two daughter cells are visible. (ns, not significant, \*\*\*,  $p < 0.001$ ; \*\*\*\*,  $p < 0.0001$ )

**Figure 8. *Ex vivo* culture of Malpighian tubules and ovaries.** (A) Malpighian tubules cultured at 18°C for 24h, then shifted to 29°C are still able to activate expression of nlsGFP driven by the *esg<sup>TS</sup>* system, showing that the epithelium remains healthy long-term. Images are maximum intensity projections. Scale bar is 50µm. (B) Quantification of GFP expression of progenitor cells from Malpighian tubules cultured *ex vivo*. Same cells were measured at 0, 1, and 2 days after explantation. (Dunnett's multiple comparisons test) (ns, not significant, \*\*\*\*,  $p < 0.0001$ ) (C) Stage 4 follicle growing in size and elongating over the course of 2 days *ex vivo*. (C') Selected frames showing follicle rotation. Cyan dots mark the current position of a nucleus, while yellow ones marked the position in the previous frame. Images are maximum intensity projections of the 4 center-most z-slices. See also Video 22. Scale bar is 10µm.

**Figure 2 – Figure supplement 1: *Ex vivo* temperature sensitive gene expression of GFP.** (A) Intestines explanted from flies raised at 18°C show no GFP expression. After explantation, guts were cultured at 29°C and started to express GFP driven by the *esg<sup>TS</sup>* system. GFP channel is a maximum intensity projection. Scale bar is 200µm. (B) Intestines cultured at 18°C for 24h, then shifted to 29°C are still able to activate expression of nlsGFP, showing that the epithelium remains healthy long-term. Images are maximum intensity projections. Scale bar is 50µm.

**Figure 3 – Figure Supplement 1: Damage response to SDS feeding *in vivo*.** (A) Images of intestines dissected and stained after being fed a control diet for 24h or SDS 0.2%-laced food for 18h then sucrose 0.05% for 6h or SDS 0.2%-laced food for 18h, sucrose 0.05% for 6h, then clean food for 24h or 48h (recovery phase). Intestines were fixed with PFA 6%, then stained with DAPI and an anti-GFP antibody, then mounted and imaged. Similarly to the *ex vivo* experiment (see Figure 3), many large GFP-dim cells can be seen after SDS treatment. Images are maximum intensity projections. Scale bar is 50µm. (B) Quantification of GFP<sup>+</sup> cells' nuclear area of intestines treated as in panel (A) showing the significant appearance of GFP<sup>+</sup> cells with large nuclei after SDS-treatment (Kruskal-Wallis test and Dunn's multiple comparisons test). (C) Phospho-Ser 10-Histone 3 (pH3) staining quantification of intestines treated as in panel (A). As observed in the *ex vivo* experiment (see Figure 3), mitoses are only detectable at a late time-point (One-way Anova and Tukey multiple comparisons test). (ns, not significant, \*\*\*\*,  $p < 0.0001$ )

**Figure 3 – Figure Supplement 2: Tissue repair in midguts damaged *ex vivo*.** (A) Diagram depicting the laceration of midgut tissues with a tungsten needle. (B) Time-lapse of an intestine expressing GFP via *esg*<sup>TS</sup> driver and damaged with a tungsten needle (white arrowhead at time-point 0h). Note the gradual replacement of the epithelium by the proliferation/differentiation of GFP<sup>+</sup> progenitor cells. Images are maximum intensity projections. See also Video 8. Scale bar is 50µm. (C) Example of stem cell dividing upon tissue damage from the intestine shown in panel B. Scale bar is 5µm. (D) Undamaged intestine expressing only low levels of upd3 (green). Images are maximum intensity projections. See also Video 9. Scale bar is 50µm. (E) Intestine damaged with the protocol described in panel (A) showing strong activation of the upd3 reporter (green) at the damaged area (marked by the yellow arrowhead). Images are maximum intensity projections. See also Video 10. Scale bar is 50µm.

**Figure 3 – Figure Supplement 3: *Notch* knock-down induces tumorigenesis *ex vivo*.** (A) Undamaged intestine expressing N<sup>RNAi</sup> under the *esg*<sup>TS</sup> driver system showing no tumorigenesis. Images are maximum intensity projections. See also Video 11. Scale bar is 20µm. (B) Intestine expressing N<sup>RNAi</sup> under the *esg*<sup>TS</sup>

driver system accidentally damaged during dissection. The damaged area (yellow ellipses) shows massive cell death. In response, *esg*<sup>+</sup> progenitor cells started to proliferate (see full and dashed yellow rectangles for examples, matching each between frames). Unlike in normal damage conditions, progenitor cells failed to differentiate (compare to Figure 3B). Images are maximum intensity projections. See also Video 12. Scale bar is 20µm.

**Figure 7 – Supplement 1. Lack of effect of genotype and time-point after mitosis on cell motility.** For all graphs, red and blue denote data from dividing and non-dividing progenies of non-co-dividing siblings, respectively, purple refers to data from all cells in non-co-dividing pairs, while green refers to data from co-dividing siblings. (A) The genotype used to promote ISC proliferation does not result in differences in cell motility in the dividing (red) or non-dividing (blue) cells from non-co-dividing siblings (Two-way Anova and Tukey multiple comparisons test). (B-D) Cell motility calculated as the distance travelled by a cell between two subsequent time-points. X-axis indicates the time passed from the first appearance of a cell. Cell motility remains constant across time for the dividing (B), non-dividing (C) cells in non-co-dividing siblings, as well as for co-dividing cells (D) (Mixed-effects analysis was used instead of Anova to account for missing values due to cells proliferating and errors during image registration. Tukey's test was used for multiple comparisons). (E) No difference in cell motility was found between dividing (red) and non-dividing (blue) cells in non-co-dividing siblings and co-dividing pairs (green). (F) Movements of cells relative to their sisters for co-dividing and non-co-dividing pairs. Only the first 6 time-points after the first appearance of each pair was used for this analysis (Mann-Whitney test). (ns, not significant, \*,  $p < 0.05$ )

## **SUPPLEMENTARY DATA**

**Supplementary File 1: Modified Schneider's medium and stock solutions recipes.**

871 **Supplementary File 2: Nuclear area and nlsGFP measurements for lineages from *Ras*<sup>G12V</sup> or *stg* and**  
872 ***CycE* over-expressing midguts.**

873 **Video 1: Dissection technique to minimize damage during midgut explantation.** See also Figure 1 and  
874 methods section.

875 **Video 2: 72h live-imaging of an undamaged intestine expressing a lineage tracing system under *esg*<sup>TS</sup>**  
876 **driver.** Maximum intensity projection. See also Figure 2C. Scale bar is 5µm.

877 **Video 3: Example of visceral muscle peristaltic movements after 3 days *ex vivo*.** Intestine was cultured  
878 in the presence of the calcium blocker isradipine. After 2-3 days in culture, the effect of the drug  
879 dissipates and the visceral muscle restarts its regular peristaltic movements. Scale bar is 50µm.

880 **Video 4: 48h live-imaging of a healthy intestine expressing *His2Av.mRFP* (red) and *esg*<sup>TS</sup>-driven nlsGFP**  
881 **(Green) induced 24h prior to imaging.** Maximum intensity projection. See also Figure 3A. Scale bar is  
882 20µm.

883 **Video 5: 48h live-imaging of an intestine from a SDS-fed fly expressing *His2Av.mRFP* (red) and *esg*<sup>TS</sup>-**  
884 **driven nlsGFP (Green) induced 24h prior to imaging.** Maximum intensity projection. See also Figure 3B.  
885 Scale bar is 20µm.

886 **Video 6: detailed view of Video 5 showing a progenitor cell (white outline) differentiating and**  
887 **replacing dying enterocytes (yellow circles) in an intestine from a SDS-fed fly expressing *His2Av.mRFP***  
888 **(red) and *esg*<sup>TS</sup>-driven nlsGFP (Green) induced 24h prior to imaging.** Maximum intensity projection. See  
889 also Figure 3B'. Scale bar is 10µm.

890 **Video 7: examples of *esg*<sup>+</sup> cells from control or SDS-damaged intestines expressing *His2Av.mRFP* (red)**  
891 **and *esg*<sup>TS</sup>-driven nlsGFP (Green) induced 24h prior to imaging.** Cells of interest are always centered. See  
892 also Figure 3D-E. Scale is 5 µm.

893 **Video 8: 20h live-imaging of an intestine expressing *esg*-driven nlsGFP (right) damaged by needle poke**  
894 **10' prior to imaging.** Maximum intensity projection. See also Figure 3 – figure supplement 2B. Scale bar  
895 is 20µm.

896 **Video 9: 24h live-imaging of an undamaged intestine expressing His2Av.mRFP (red) and upd3-driven**  
897 **GFP (green).** Maximum intensity projection. See also Figure 3 – figure supplement 2D.

898 **Video 10: 24h live-imaging of an intestine damaged using a tungsten needle and expressing**  
899 **His2Av.mRFP (red) and upd3-driven GFP (green).** Damaged area is marked by the yellow arrowhead.  
900 Maximum intensity projection. See also Figure 3 – figure supplement 2E.

901 **Video 11: 48h live-imaging of an undamaged intestine expressing His2Av.mRFP (red) and *esg*<sup>TS</sup>-driven**  
902 **nlsGFP (Green) and *N*<sup>RNAi</sup> induced 24h prior to imaging.** Maximum intensity projection. See also Figure  
903 Figure 3 – figure supplement 3A. Scale bar is 20µm.

904 **Video 12: 48h live-imaging of a damaged intestine expressing His2Av.mRFP (red) and *esg*<sup>TS</sup>-driven**  
905 **nlsGFP (Green) and *N*<sup>RNAi</sup> induced 24h prior to imaging.** Damaged area is marked by the yellow ellipses.  
906 Maximum intensity projection. See also Figure Figure 3 – figure supplement 3B. Scale bar is 20µm.

907 **Video 13: 48h live-imaging of a healthy intestine expressing His2Av.mRFP (red) and *esg*<sup>TS</sup>-driven**  
908 **nlsGFP (Green) induced after dissection.** Maximum intensity projection. See also Figure 4A. Scale bar is  
909 20µm.

910 **Video 14: 48h live-imaging of an intestine expressing His2Av.mRFP (red) and *esg*<sup>TS</sup>-driven nlsGFP**  
911 **(Green) and *Ras*<sup>G12V</sup> induced after dissection.** Maximum intensity projection. See also Figure 4B. Scale  
912 bar is 20µm.

913 **Video 15: 48h live-imaging of an intestine expressing His2Av.mRFP (red) and *esg*<sup>TS</sup>-driven nlsGFP**  
 914 **(Green), *stg*, and *CycE* induced after dissection.** Maximum intensity projection. See also Figure 4C. Scale  
 915 bar is 20µm.

916 **Video 16: Example of ISC lineage.** Arrowheads indicate cells in the lineage. Maximum intensity  
 917 projections of z-slices encompassing the cells in the lineage. See also Figure 5. Scale bar is 5µm.

918 **Video 17: Example of division giving rise to co-dividing siblings.** Arrowheads indicate cells in the  
 919 lineage, with co-dividing pair marked by green ones. Maximum intensity projections of z-slices  
 920 encompassing the cells in the lineage. See also Figure 6A. Scale bar is 5µm.

921 **Video 18: Example of division giving rise to non-co-dividing siblings.** Arrowheads indicate cells in the  
 922 lineage, with non-co-dividing pair marked by red ones. Maximum intensity projections of z-slices  
 923 encompassing the cells in the lineage. See also Figure 6C. Scale bar is 5µm.

924 **Video 19: Example of Malpighian tubule contracting after 3 days *ex vivo*.** Note that the tubule is still  
 925 connected to the midgut. To avoid inhibiting contractions, isradipine was not supplemented, resulting in  
 926 the midgut rupturing near the imaged site, releasing visible debris. Scale bar is 50µm.

927 **Video 20: Example of heart lining the dorsal side of a dissected fly abdomen beating after 10 days *ex***  
 928 ***vivo*.** Scale bar is 50µm.

929 **Video 21: Example of ovary contracting after 3 days *ex vivo*.** Scale bar is 100µm.

930 **Video 22: Example of a rotating stage 4 follicle progressing to stage 5 *ex vivo* and starting to elongate**  
 931 **along its long axis.** Left panel is a maximum intensity projection of the 3 center-most z-slices. White  
 932 dotted line indicates the plane corresponding to the cross-section shown on the right panel. The cross-  
 933 section shows the follicle rotates along its axis of elongation. See also Figure 8C. Scale bar is 10µm.



934 **Video 23: Example of high frame-rate long-term confocal imaging.** Undamaged control intestine  
935 expressing His2Av.mRFP (red) and *esg*<sup>TS</sup>-driven nlsGFP (Green) induced 24h prior to imaging. Maximum  
936 intensity projection. Scale bar is 50µm.

937 **Figure 2 – source data 1.** Raw data for Figure 2A, D, E.

938 **Figure 3 – source data 1.** Raw data for Figure 3D-G.

939 **Figure 3 – figure supplement 1 – source data 1.** Raw data for Figure 3 – figure supplement 1B-C.

940 **Figure 4 – source data 1.** Raw data for Figure 4D, F.

941 **Figure 6 – source data 1.** Raw data for Figure 6E-H.

942 **Figure 7 – source data 1.** Raw data for Figure 7A, D, F.

943 **Figure 7 – figure supplement 1 – source data 1.** Raw data for Figure 7 – figure supplement 1A-F.

944 **Figure 8 – source data 1.** Raw data for Figure 8B.

945 **Source code 1.** This Python script is used for local registration of adult *Drosophila* midgut fluorescent  
946 imaging time-lapses. Movies are converted to 8bit, normalized by subtracting mean and dividing by the  
947 standard deviation, converted to maximum intensity or focused projections, then divided in partially  
948 overlapping regions of interest (ROIs). Each ROI is then XY-registered via cross-correlation between  
949 frames and then the most in-focus Z slice is found. Finally, ROIs are exported.

950 **Source code 2.** ImageJ Macro designed for the manual tracking of cells in two-channel time-lapse images  
951 of adult *Drosophila* midguts. Images must be two-channel time-lapse z-stacks, with channels 1 and 2  
952 being His2Av.mRFP and *esg*<sup>TS</sup> > nlsGFP, respectively.

953 **Source code 3.** This Python script is used to parse files generated by the "Source code 2" ImageJ macro.  
954 First, the lineage is reconstructed based on relative cell distances between frames. For each cell in frame

955 f, a new position in frame f+1 is assigned, based on the pool of annotated cell positions in f+1. All  
956 possible permutations between f and f+1 coordinates are computed and the total distance between cell  
957 positions in frame f and their newly assigned positions in f+1 is calculated. The permutation for which  
958 this distance is minimum is then kept. If lineages are too complex (e.g. cells are moving and rearranging  
959 themselves), then the user can add two additional field to the input ".tsv" file ("CellID" and "MotherID"  
960 columns) indicating each cells ID (for each cell position) and its mother cell ID (can be stated once). The  
961 lineage data is then parsed and formatted in an easy to read format, then exported to a ".tsv" file.

962

## REFERENCES

1. Ohlstein, B. & Spradling, A. The adult *Drosophila* posterior midgut is maintained by pluripotent stem cells. *Nature* **439**, 470–474 (2006).
2. Micchelli, C. A. & Perrimon, N. Evidence that stem cells reside in the adult *Drosophila* midgut epithelium. *Nature* **439**, 475–479 (2006).
3. Jiang, H. *et al.* Cytokine/Jak/Stat signaling mediates regeneration and homeostasis in the *Drosophila* midgut. *Cell* **137**, 1343–1355 (2009).
4. Beebe, K., Lee, W.-C. & Micchelli, C. A. JAK/STAT signaling coordinates stem cell proliferation and multilineage differentiation in the *Drosophila* intestinal stem cell lineage. *Dev. Biol.* **338**, 28–37 (2010).
5. Patel, P. H. *et al.* Damage sensing by a Nox-Ask1-MKK3-p38 signaling pathway mediates regeneration in the adult *Drosophila* midgut. *Nat. Commun.* **10**, 1–14 (2019).
6. Sato, T. *et al.* Single Lgr5 stem cells build crypt-villus structures in vitro without a mesenchymal niche. *Nature* **459**, 262–265 (2009).
7. Robb, J. A. Maintenance of imaginal discs of *Drosophila* in chemically defined media. *J. Cell Biol.* **41**, 876–885 (1969).
8. Zartman, J., Restrepo, S. & Basler, K. A high-throughput template for optimizing *Drosophila* organ culture with response-surface methods. *Development* **140**, 667–674 (2013).
9. Handke, B., Szabad, J., Lidsky, P. V., Hafen, E. & Lehner, C. F. Towards Long Term Cultivation of *Drosophila* Wing Imaginal Discs In Vitro. *PLOS ONE* **9**, e107333 (2014).
10. Tsao, C.-K., Ku, H.-Y., Lee, Y.-M., Huang, Y.-F. & Sun, Y. H. Long Term Ex Vivo Culture and Live Imaging of *Drosophila* Larval Imaginal Discs. *PLOS ONE* **11**, e0163744 (2016).
11. Strassburger, K. *et al.* Oxygenation and adenosine deaminase support growth and proliferation of ex vivo cultured *Drosophila* wing imaginal discs. *Development* **144**, 2529–2538 (2017).
12. Siller, K. H., Serr, M., Steward, R., Hays, T. S. & Doe, C. Q. Live Imaging of *Drosophila* Brain Neuroblasts Reveals a Role for Lis1/Dynactin in Spindle Assembly and Mitotic Checkpoint Control. *Mol. Biol. Cell* **16**, 5127–5140 (2005).
13. Rabinovich, D., Mayseless, O. & Schuldiner, O. Long term ex vivo culturing of *Drosophila* brain as a method to live image pupal brains: insights into the cellular mechanisms of neuronal remodeling. *Front. Cell. Neurosci.* **0**, (2015).
14. Fichelson, P. *et al.* Live-imaging of single stem cells within their niche reveals that a U3snoRNP component segregates asymmetrically and is required for self-renewal in *Drosophila*. *Nat. Cell Biol.* **11**, 685–693 (2009).

996 15. Morris, L. X. & Spradling, A. C. Long-term live imaging provides new insight into stem cell  
997 regulation and germline-soma coordination in the *Drosophila* ovary. *Dev. Camb. Engl.* **138**, 2207–2215  
998 (2011).

999 16. Reilein, A., Cimetta, E., Tandon, N. M., Kalderon, D. & Vunjak-Novakovic, G. Live imaging of stem  
1000 cells in the germarium of the *Drosophila* ovary using a reusable gas-permeable imaging chamber. *Nat.*  
1001 *Protoc.* **13**, 2601–2614 (2018).

1002 17. Cheng, J. & Hunt, A. J. Time-lapse Live Imaging of Stem Cells in *Drosophila* Testis. *Curr. Protoc.*  
1003 *Stem Cell Biol.* **CHAPTER**, Unit-2E.2 (2009).

1004 18. Deng, H., Gerencser, A. A. & Jasper, H. Signal integration by Ca<sup>2+</sup> regulates intestinal stem cell  
1005 activity. *Nature* **528**, 212–217 (2015).

1006 19. Xu, C., Luo, J., He, L., Montell, C. & Perrimon, N. Oxidative stress induces stem cell proliferation  
1007 via TRPA1/RyR-mediated Ca<sup>2+</sup> signaling in the *Drosophila* midgut. *eLife* **6**, e22441 (2017).

1008 20. He, L., Si, G., Huang, J., Samuel, A. D. T. & Perrimon, N. Mechanical regulation of stem cell  
1009 differentiation through stretch-activated Piezo channel. *Nature* **555**, 103–106 (2018).

1010 21. Martin, J. L. *et al.* Long-term live imaging of the *Drosophila* adult midgut reveals real-time  
1011 dynamics of division, differentiation and loss. *eLife* **7**, e36248 (2018).

1012 22. Hu, D. J.-K. & Jasper, H. Control of Intestinal Cell Fate by Dynamic Mitotic Spindle Repositioning  
1013 Influences Epithelial Homeostasis and Longevity. *Cell Rep.* **28**, 2807-2823.e5 (2019).

1014 23. Pasco, M. Y. & Léopold, P. High Sugar-Induced Insulin Resistance in *Drosophila* Relies on the  
1015 Lipocalin Neural Lazarillo. *PLoS ONE* **7**, e36583 (2012).

1016 24. Dus, M., Ai, M. & Suh, G. S. B. Taste-independent nutrient selection is mediated by a brain-  
1017 specific Na<sup>+</sup>/solute co-transporter in *Drosophila*. *Nat. Neurosci.* **16**, 526–528 (2013).

1018 25. Park, S. *et al.* A Genetic Strategy to Measure Circulating *Drosophila* Insulin Reveals Genes  
1019 Regulating Insulin Production and Secretion. *PLoS Genet.* **10**, e1004555 (2014).

1020 26. Tennessen, J. M., Barry, W., Cox, J. & Thummel, C. S. Methods for studying metabolism in  
1021 *Drosophila*. *Methods San Diego Calif* **68**, 105–115 (2014).

1022 27. Matsushita, R. & Nishimura, T. Trehalose metabolism confers developmental robustness and  
1023 stability in *Drosophila* by regulating glucose homeostasis. *Commun. Biol.* **3**, 1–12 (2020).

1024 28. Singleton, K. & Woodruff, R. I. The Osmolarity of Adult *Drosophila* Hemolymph and Its Effect on  
1025 Oocyte-Nurse Cell Electrical Polarity. *Dev. Biol.* **161**, 154–167 (1994).

1026 29. Naikhwah, W. & O'Donnell, M. J. Salt stress alters fluid and ion transport by Malpighian tubules  
1027 of *Drosophila melanogaster*: evidence for phenotypic plasticity. *J. Exp. Biol.* **214**, 3443–3454 (2011).

1028 30. MacMillan, H. A. *et al.* Parallel ionoregulatory adjustments underlie phenotypic plasticity and  
1029 evolution of *Drosophila* cold tolerance. *J. Exp. Biol.* **218**, 423–432 (2015).

1030 31. MacMillan, H. A., Andersen, J. L., Davies, S. A. & Overgaard, J. The capacity to maintain ion and  
1031 water homeostasis underlies interspecific variation in *Drosophila* cold tolerance. *Sci. Rep.* **5**, 1–11 (2015).

1032 32. Olsson, T. *et al.* Hemolymph metabolites and osmolality are tightly linked to cold tolerance of  
1033 *Drosophila* species: a comparative study. *J. Exp. Biol.* **219**, 2504–2513 (2016).

1034 33. Schneider, I. DIFFERENTIATION OF LARVAL DROSOPHILA EYE-ANTENNAL DISCS IN VITRO. *J. Exp.*  
1035 *Zool.* **156**, 91–103 (1964).

1036 34. Schneider, I. Histology of larval eye-antennal disks and cephalic ganglia of *Drosophila* cultured in  
1037 vitro. *J. Embryol. Exp. Morphol.* **15**, 271–279 (1966).

1038 35. Schneider, I. Cell lines derived from late embryonic stages of *Drosophila melanogaster*. *J.*  
1039 *Embryol. Exp. Morphol.* **27**, 353–365 (1972).

1040 36. Schneider, I. & Blumenthal, A. B. *Drosophila* cell and tissue culture. in *The Genetics and Biology*  
1041 *of Drosophila*. 265–315 (1978).

1042 37. Davis, K. T. & Shearn, A. In Vitro Growth of Imaginal Disks from *Drosophila melanogaster*.  
1043 *Science* **196**, 438–440 (1977).

1044 38. Britton, J. S. & Edgar, B. A. Environmental control of the cell cycle in *Drosophila*: nutrition  
1045 activates mitotic and endoreplicative cells by distinct mechanisms. *Dev. Camb. Engl.* **125**, 2149–2158  
1046 (1998).

1047 39. Icha, J., Weber, M., Waters, J. C. & Norden, C. Phototoxicity in live fluorescence microscopy, and  
1048 how to avoid it. *BioEssays* **39**, 1700003 (2017).

1049 40. Ezeriņa, D., Takano, Y., Hanaoka, K., Urano, Y. & Dick, T. P. N-Acetyl Cysteine Functions as a Fast-  
1050 Acting Antioxidant by Triggering Intracellular H<sub>2</sub>S and Sulfane Sulfur Production. *Cell Chem. Biol.* **25**,  
1051 447–459.e4 (2018).

1052 41. Wu, X. *et al.* Citrate reduced oxidative damage in stem cells by regulating cellular redox signaling  
1053 pathways and represent a potential treatment for oxidative stress-induced diseases. *Redox Biol.* **21**,  
1054 101057 (2019).

1055 42. *Drosophila* Cells in Culture (Second Edition). in *Drosophila Cells in Culture (Second Edition)* (eds.  
1056 Echalié, G., Perrimon, N. & Mohr, S. E.) iv (Academic Press, 2018). doi:10.1016/B978-0-12-809473-  
1057 0.00012-9.

1058 43. Brand, A. H. & Perrimon, N. Targeted gene expression as a means of altering cell fates and  
1059 generating dominant phenotypes. *Dev. Camb. Engl.* **118**, 401–415 (1993).

1060 44. McGuire, S. E. Spatiotemporal Rescue of Memory Dysfunction in *Drosophila*. *Science* **302**, 1765–  
1061 1768 (2003).

1062 45. Liang, J., Balachandra, S., Ngo, S. & O’Brien, L. E. Feedback regulation of steady-state epithelial  
1063 turnover and organ size. *Nature* **548**, 588–591 (2017).

1064 46. Li, Q. *et al.* Ingestion of Food Particles Regulates the Mechanosensing Misshapen-Yorkie  
1065 Pathway in *Drosophila* Intestinal Growth. *Dev. Cell* **45**, 433–449.e6 (2018).

1066 47. Amcheslavsky, A., Jiang, J. & Ip, Y. T. Tissue Damage-Induced Intestinal Stem Cell Division in  
1067 *Drosophila*. *Cell Stem Cell* **4**, 49–61 (2009).

1068 48. Hu, D. J.-K., Yun, J., Elstrott, J. & Jasper, H. Non-canonical Wnt signaling promotes directed  
1069 migration of intestinal stem cells to sites of injury. *Nat. Commun.* **12**, 7150 (2021).

1070 49. Patel, P. H., Dutta, D. & Edgar, B. A. Niche Appropriation by *Drosophila* Intestinal Stem Cell  
1071 Tumors. *Nat. Cell Biol.* **17**, 1182–1192 (2015).

1072 50. Buchon, N., Broderick, N. A., Poidevin, M., Pradervand, S. & Lemaitre, B. *Drosophila* intestinal  
1073 response to bacterial infection: activation of host defense and stem cell proliferation. *Cell Host Microbe*  
1074 **5**, 200–211 (2009).

1075 51. Reiff, T. *et al.* Notch and EGFR regulate apoptosis in progenitor cells to ensure gut homeostasis  
1076 in *Drosophila*. *EMBO J.* **38**, e101346 (2019).

1077 52. de Navascués, J. *et al.* *Drosophila* midgut homeostasis involves neutral competition between  
1078 symmetrically dividing intestinal stem cells. *EMBO J.* **31**, 2473–2485 (2012).

1079 53. Lin, G., Xu, N. & Xi, R. Paracrine Wingless signalling controls self-renewal of *Drosophila* intestinal  
1080 stem cells. *Nature* **455**, 1119–1123 (2008).

1081 54. Shaw, R. L. *et al.* The Hippo pathway regulates intestinal stem cell proliferation during  
1082 *Drosophila* adult midgut regeneration. *Dev. Camb. Engl.* **137**, 4147–4158 (2010).

1083 55. Strand, M. & Micchelli, C. A. Quiescent gastric stem cells maintain the adult *Drosophila* stomach.  
1084 *Proc. Natl. Acad. Sci.* **108**, 17696–17701 (2011).

1085 56. Ohlstein, B. & Spradling, A. Multipotent *Drosophila* Intestinal Stem Cells Specify Daughter Cell  
1086 Fates by Differential Notch Signaling. *Science* **315**, 988–992 (2007).

1087 57. Apidianakis, Y., Pitsouli, C., Perrimon, N. & Rahme, L. Synergy between bacterial infection and  
1088 genetic predisposition in intestinal dysplasia. *Proc. Natl. Acad. Sci. U. S. A.* **106**, 20883–20888 (2009).

1089 58. Buchon, N., Broderick, N. A., Kuraishi, T. & Lemaitre, B. *Drosophila* EGFR pathway coordinates  
1090 stem cell proliferation and gut remodeling following infection. *BMC Biol.* **8**, 152 (2010).

1091 59. Biteau, B. & Jasper, H. EGF signaling regulates the proliferation of intestinal stem cells in  
1092 *Drosophila*. *Development* **138**, 1045–1055 (2011).

1093 60. Jiang, H., Grenley, M. O., Bravo, M.-J., Blumhagen, R. Z. & Edgar, B. A. EGFR/Ras/MAPK signaling  
1094 mediates adult midgut epithelial homeostasis and regeneration in *Drosophila*. *Cell Stem Cell* **8**, 84–95  
1095 (2011).

1096 61. Jin, Y. *et al.* EGFR/Ras Signaling Controls *Drosophila* Intestinal Stem Cell Proliferation via  
1097 Capicua-Regulated Genes. *PLoS Genet.* **11**, e1005634 (2015).

1098 62. Xiang, J. *et al.* EGFR-dependent TOR-independent endocycles support *Drosophila* gut epithelial  
1099 regeneration. *Nat. Commun.* **8**, 15125 (2017).

1100 63. Chen, J. *et al.* Transient Scute activation via a self-stimulatory loop directs enteroendocrine cell  
1101 pair specification from self-renewing intestinal stem cells. *Nat. Cell Biol.* **20**, 152–161 (2018).

1102 64. Tian, A. *et al.* Re-entry into mitosis and regeneration of intestinal stem cells through enteroblast  
1103 dedifferentiation in *Drosophila* midguts. 2021.11.22.469515 Preprint at  
1104 <https://doi.org/10.1101/2021.11.22.469515> (2021).

1105 65. Kohlmaier, A. *et al.* Src kinase function controls progenitor cell pools during regeneration and  
1106 tumor onset in the *Drosophila* intestine. *Oncogene* **34**, 2371–2384 (2015).

1107 66. Goulas, S., Conder, R. & Knoblich, J. A. The Par complex and integrins direct asymmetric cell  
1108 division in adult intestinal stem cells. *Cell Stem Cell* **11**, 529–540 (2012).

1109 67. Singh, S. R., Liu, W. & Hou, S. X. The Adult *Drosophila* Malpighian Tubules Are Maintained by  
1110 Pluripotent Stem Cells. *Cell Stem Cell* **1**, 191–203 (2007).

1111 68. Wang, C. & Spradling, A. C. An abundant quiescent stem cell population in *Drosophila*  
1112 Malpighian tubules protects principal cells from kidney stones. *eLife* **9**, e54096 (2020).

1113 69. Cetera, M. *et al.* Epithelial rotation promotes the global alignment of contractile actin bundles  
1114 during *Drosophila* egg chamber elongation. *Nat. Commun.* **5**, 5511 (2014).

1115 70. Li, Z., Zhang, Y., Han, L., Shi, L. & Lin, X. Trachea-Derived Dpp Controls Adult Midgut Homeostasis  
1116 in *Drosophila*. *Dev. Cell* **24**, 133–143 (2013).

1117 71. Choi, N. H., Lucchetta, E. & Ohlstein, B. Nonautonomous regulation of *Drosophila* midgut stem  
1118 cell proliferation by the insulin-signaling pathway. *Proc. Natl. Acad. Sci.* **108**, 18702–18707 (2011).

1119 72. O’Brien, L. E., Soliman, S. S., Li, X. & Bilder, D. Altered Modes of Stem Cell Division Drive Adaptive  
1120 Intestinal Growth. *Cell* **147**, 603–614 (2011).

1121 73. Jin, Y. *et al.* Intestinal Stem Cell Pool Regulation in *Drosophila*. *Stem Cell Rep.* **8**, 1479–1487  
1122 (2017).

1123 74. Dutta, D. *et al.* Regional Cell-Specific Transcriptome Mapping Reveals Regulatory Complexity in  
1124 the Adult *Drosophila* Midgut. *Cell Rep.* **12**, 346–358 (2015).

1125 75. Hung, R.-J. *et al.* A cell atlas of the adult *Drosophila* midgut. *Proc. Natl. Acad. Sci. U. S. A.* **117**,  
1126 1514–1523 (2020).

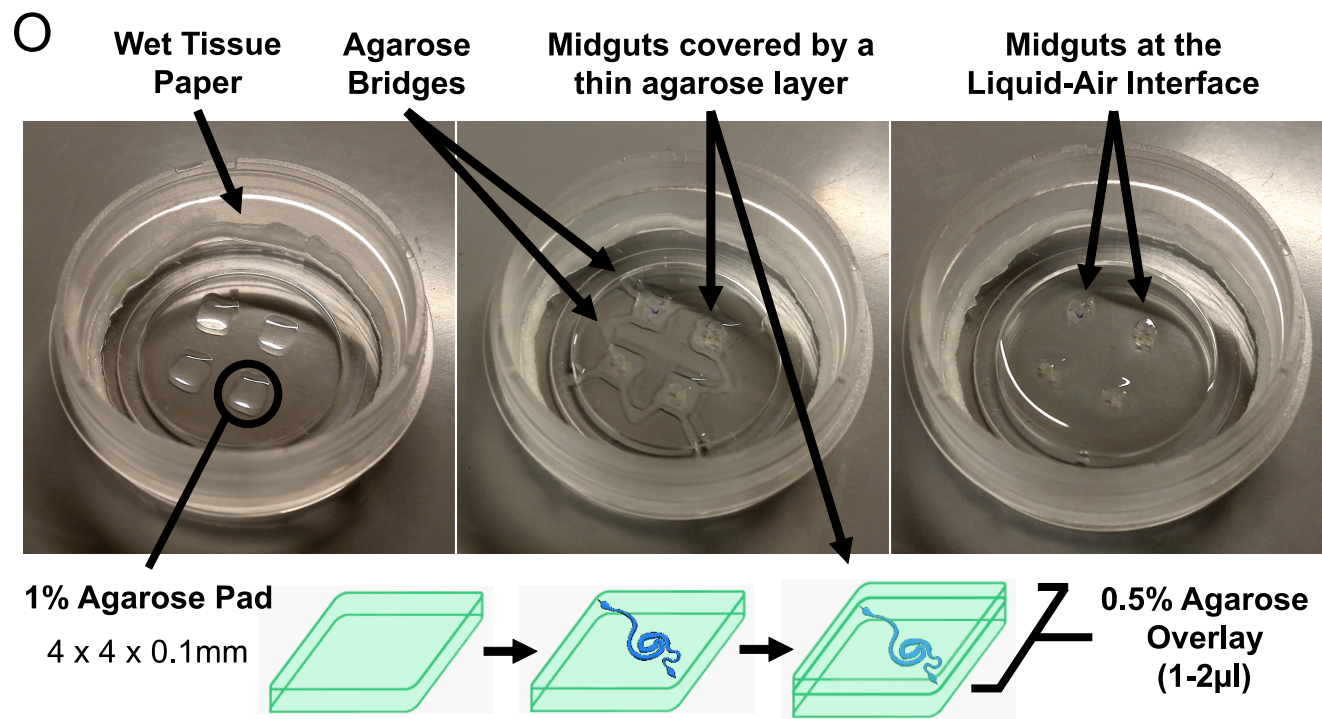
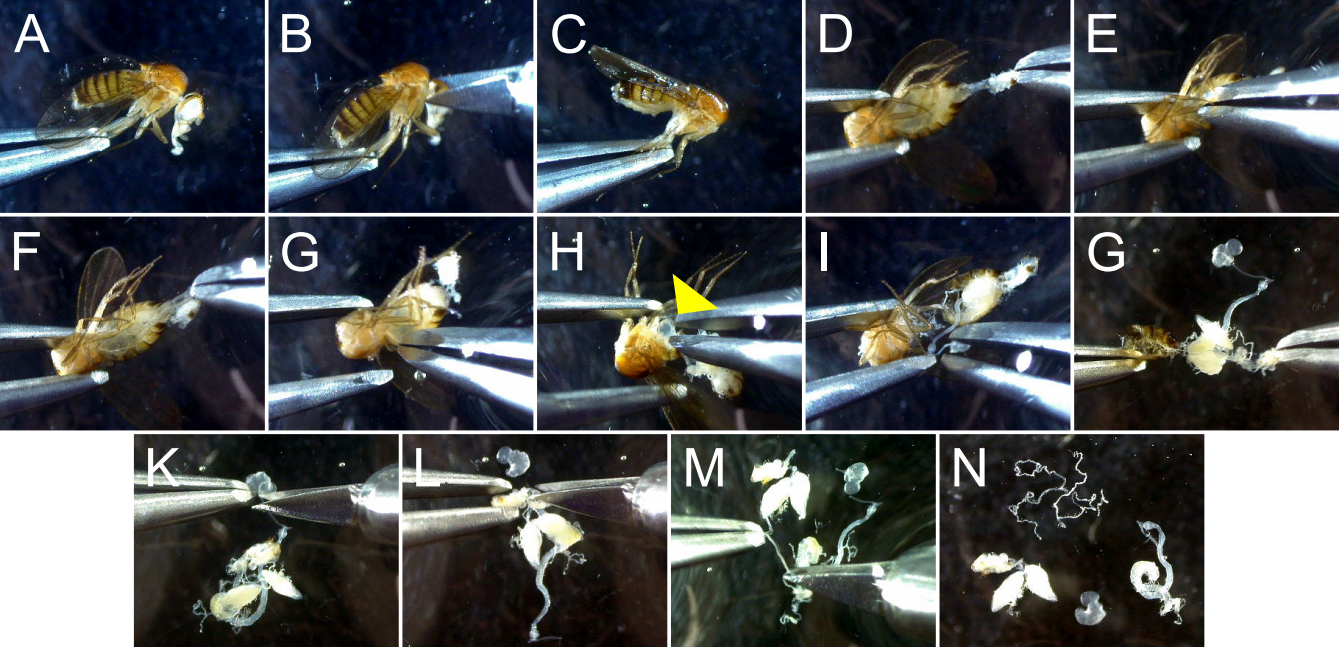
1127 76. Prior, I. A., Hood, F. E. & Hartley, J. L. The Frequency of Ras Mutations in Cancer. *Cancer Res.* **80**,  
1128 2969–2974 (2020).

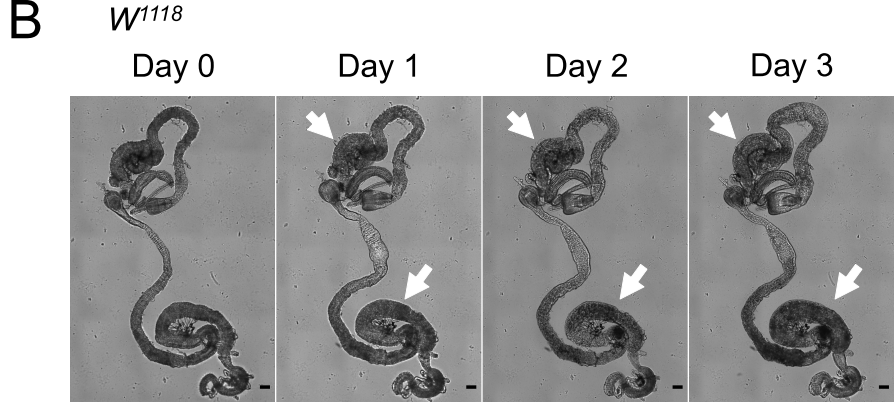
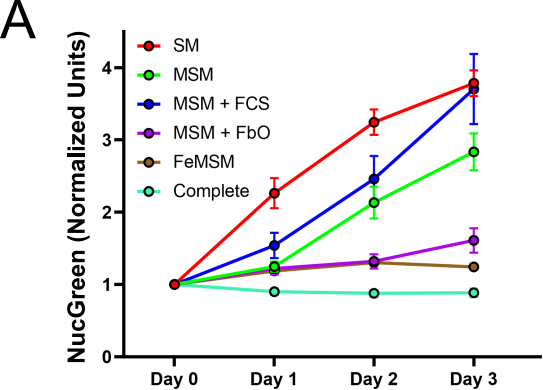
1129 77. O’Keefe, D. D., Prober, D. A., Moyle, P. S., Rickoll, W. L. & Edgar, B. A. Egfr/Ras signaling  
1130 regulates DE-cadherin/Shotgun localization to control vein morphogenesis in the *Drosophila* wing. *Dev.*  
1131 *Biol.* **311**, 25–39 (2007).

1132 78. Robertson, F., Pinal, N., Fichelson, P. & Pichaud, F. Atonal and EGFR signalling orchestrate rok-  
1133 and Drak-dependent adherens junction remodelling during ommatidia morphogenesis. *Dev. Camb. Engl.*  
1134 **139**, 3432–3441 (2012).

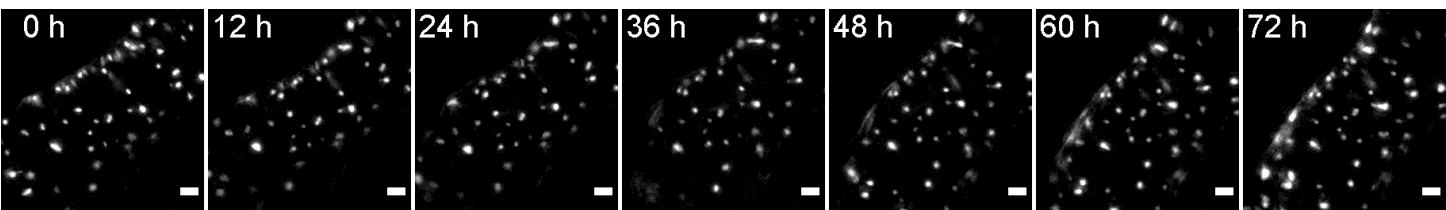
- 1135 79. Ahmed, S. M. H. *et al.* Fitness trade-offs incurred by ovary-to-gut steroid signalling in *Drosophila*.  
1136 *Nature* **584**, 415–419 (2020).
- 1137 80. Hudry, B., Khadayate, S. & Miguel-Aliaga, I. The sexual identity of adult intestinal stem cells  
1138 controls organ size and plasticity. *Nature* **530**, 344–348 (2016).
- 1139 81. Hudry, B. *et al.* Sex Differences in Intestinal Carbohydrate Metabolism Promote Food Intake and  
1140 Sperm Maturation. *Cell* **178**, 901-918.e16 (2019).
- 1141 82. Otsu, N. A Threshold Selection Method from Gray-Level Histograms. *IEEE Trans. Syst. Man*  
1142 *Cybern.* **9**, 62–66 (1979).
- 1143



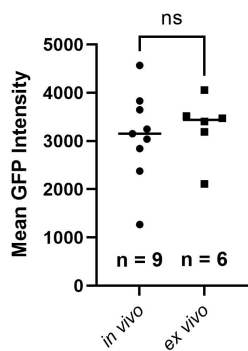
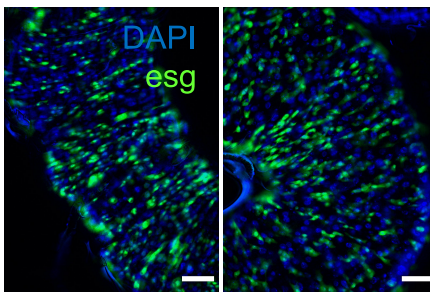




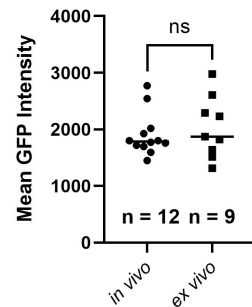
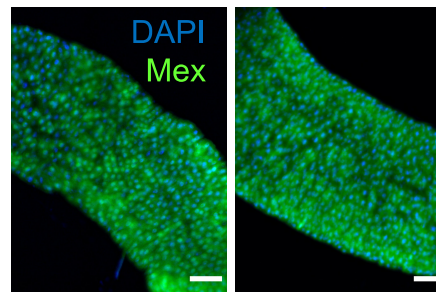
**C** *esg-Gal4 tubGal80ts UAS-GFP;*  
*UAS-flp Act>CD2>Gal4*



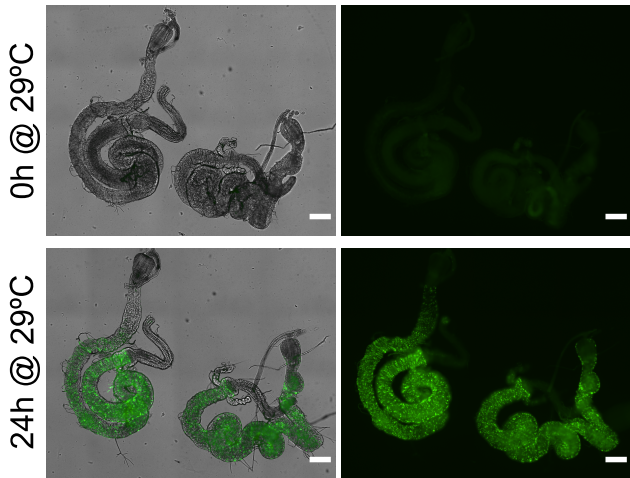
**D** *esg-Gal4 Tub-Gal80<sup>TS</sup> UAS-GFP*  
29°C 24h  
*in vivo* *ex vivo*



**E** *mex-Gal4 Tub-Gal80<sup>TS</sup> UAS-GFP*  
29°C 24h  
*in vivo* *ex vivo*

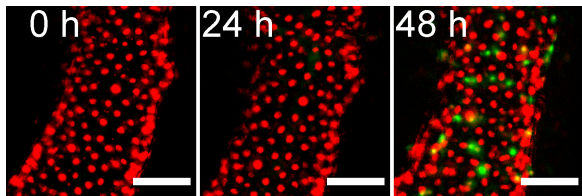


**A** *esg-Gal4 Tub-Gal80<sup>TS</sup> UAS-GFP*

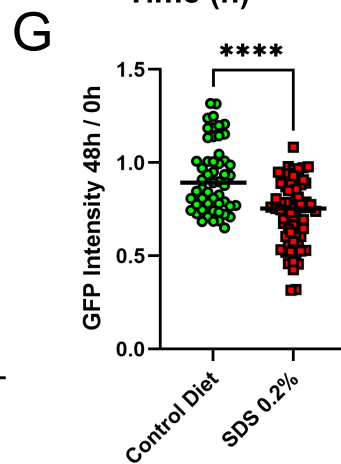
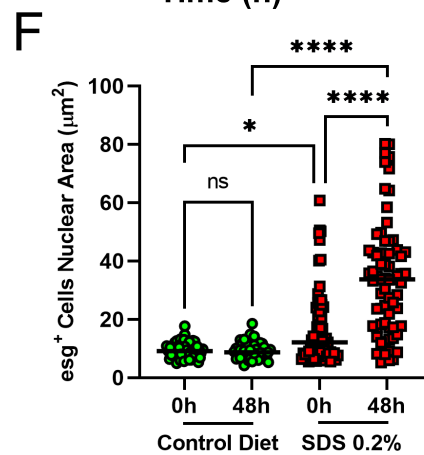
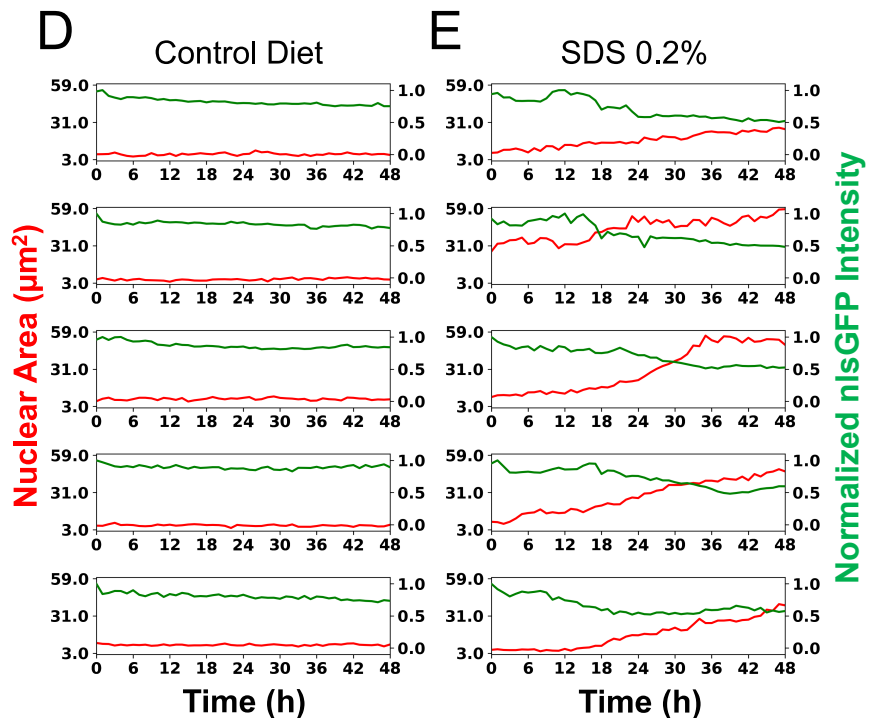
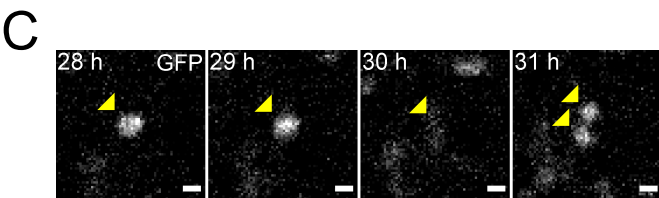
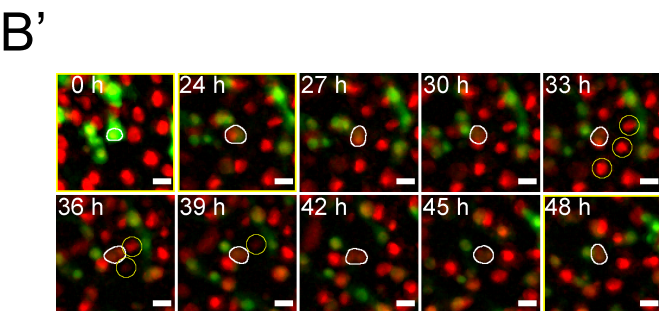
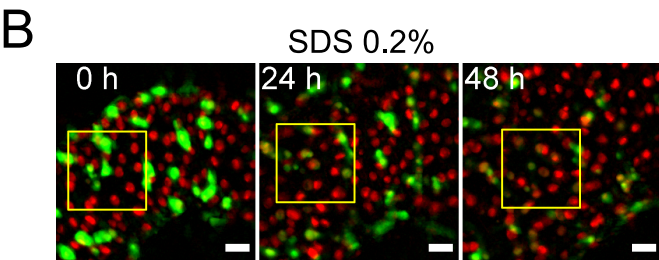
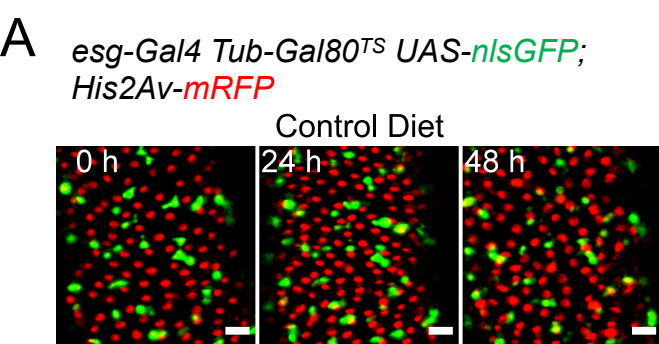


**B** *esg-Gal4 Tub-Gal80<sup>TS</sup> UAS-nlsGFP; His2Av-mRFP*

0h 18°C 24h 29°C 48h

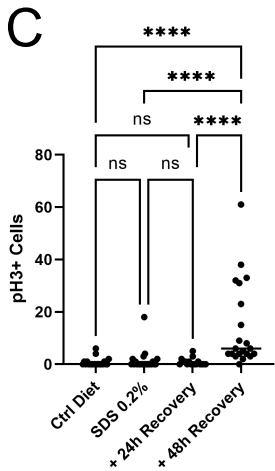
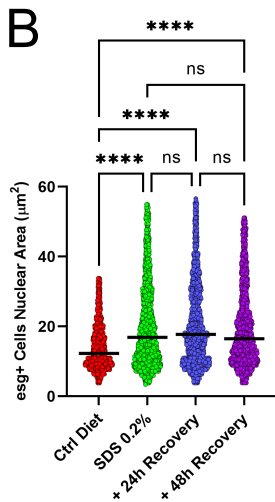
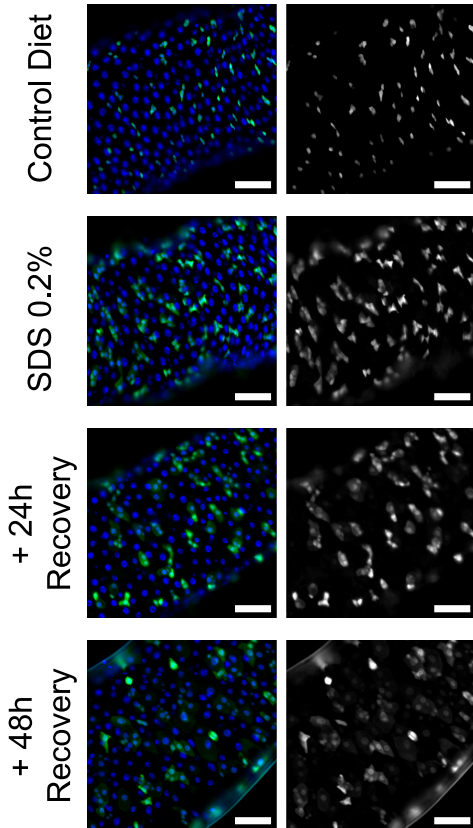




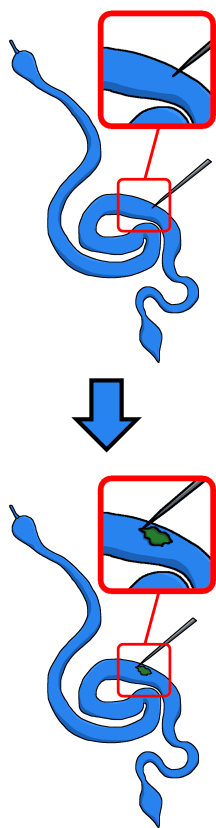


**A** *esg-Gal4 Tub-Gal80<sup>TS</sup> UAS-nlsGFP;  
His2Av-mRFP*

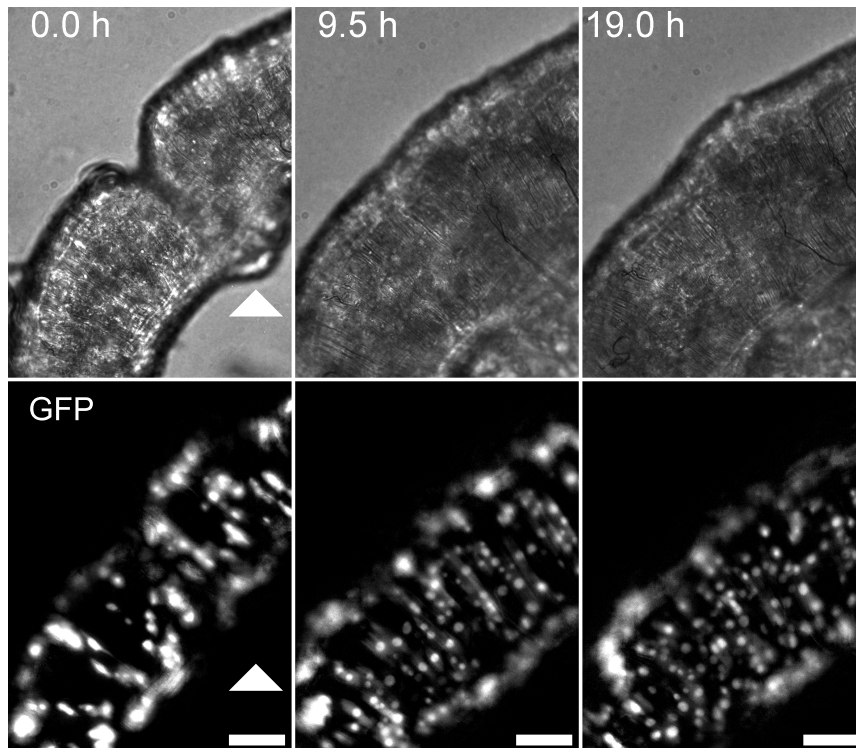
DAPI GFP



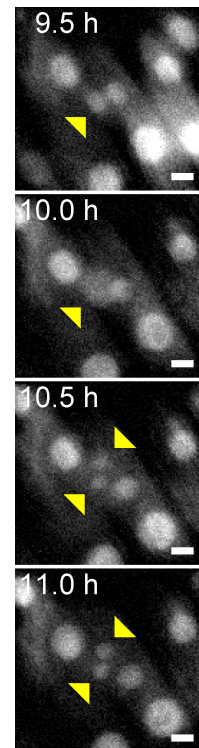
A



B

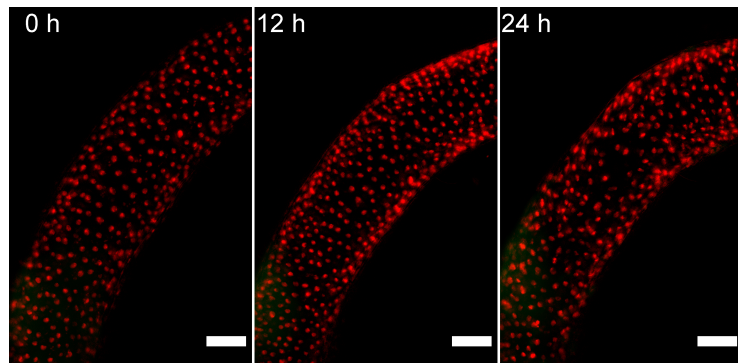
*esg-Gal4 UAS-nlsGFP*

C



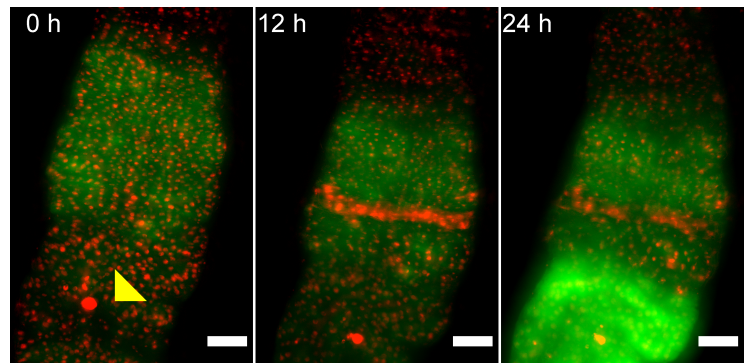
D *upd3-Gal4 UAS-GFP*;  
*His2Av-mRFP*

Undamaged



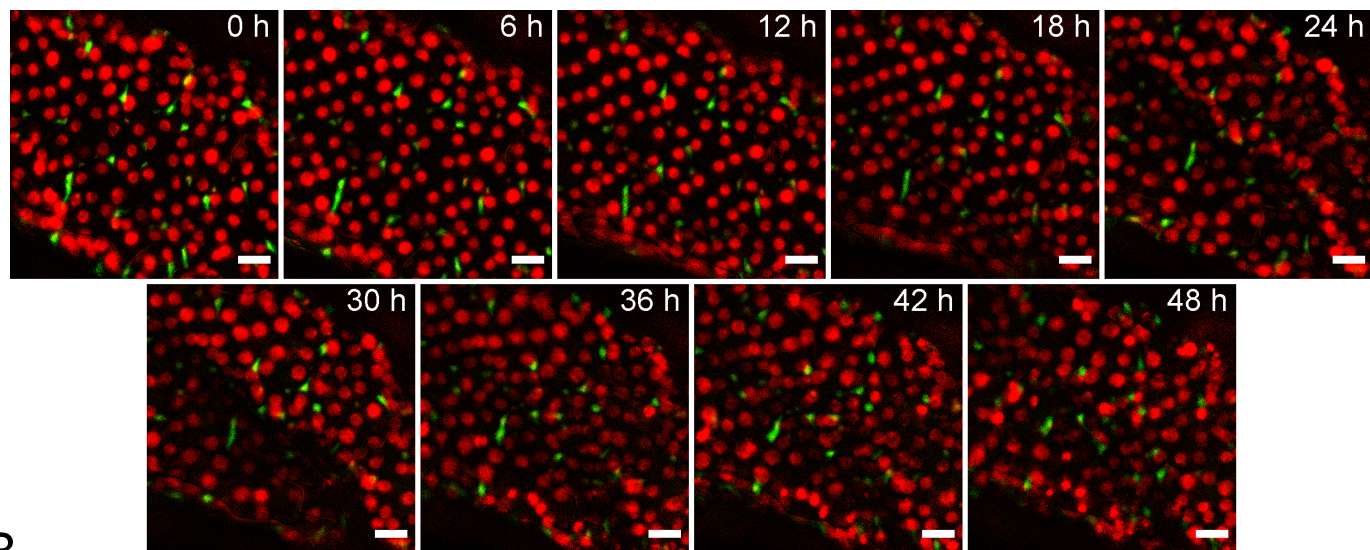
E

Needle poked

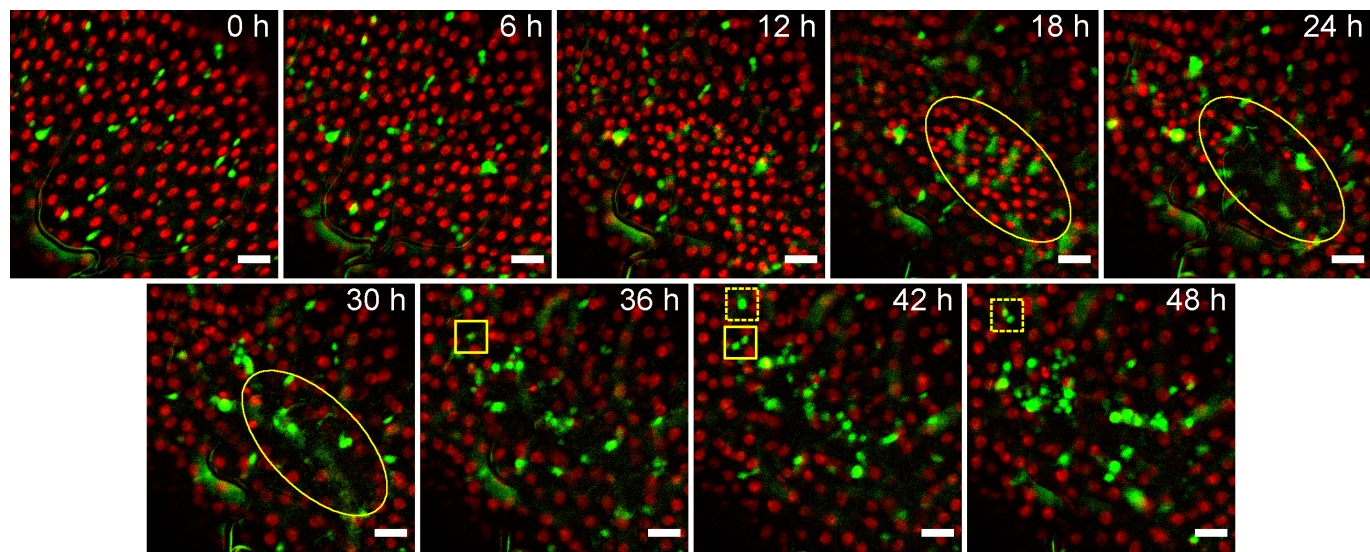




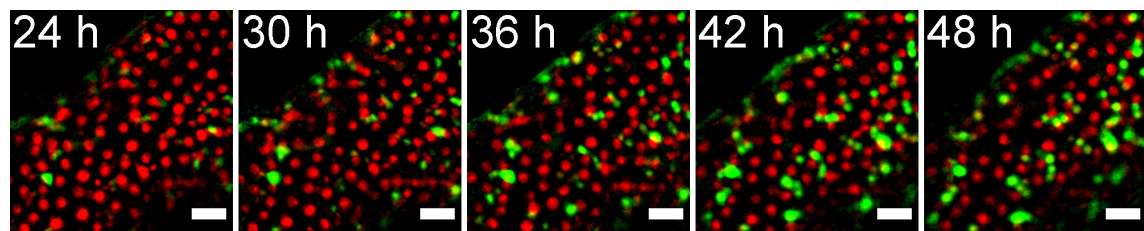
**A** *esg-Gal4 Tub-Gal80<sup>TS</sup> UAS-nlsGFP;*  
*His2Av-mRFP / UAS-Notch<sup>RNAi</sup>*



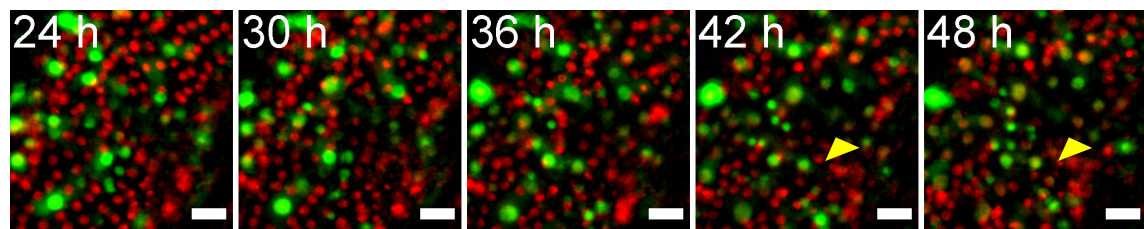
**B**



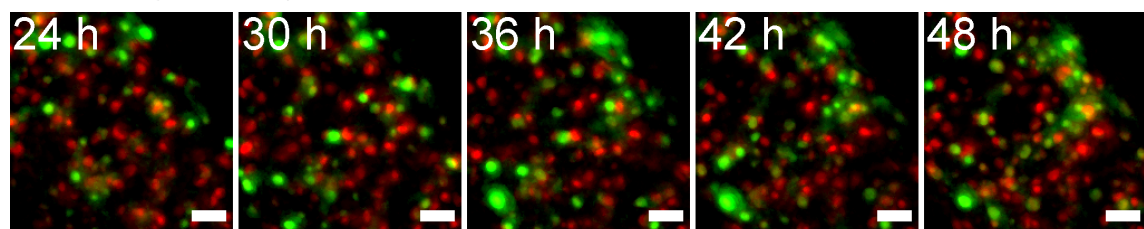
**A** *esg-Gal4 Tub-Gal80<sup>TS</sup> UAS-nlsGFP;*  
*His2Av-mRFP*





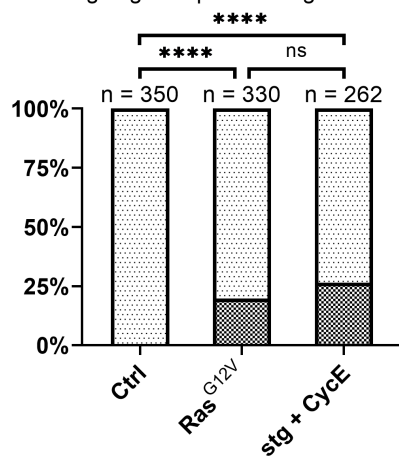
**B** *> UAS-Ras<sup>G12V</sup>*





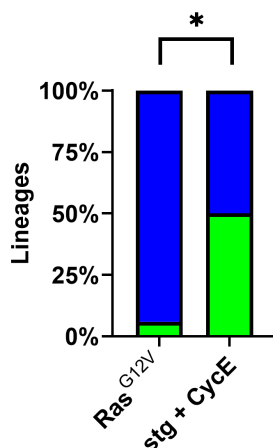
**C** *> UAS-stg, UAS-CycE*



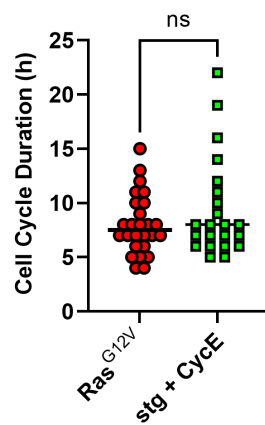
**D**  starting *esg*<sup>+</sup> proliferating cells  
 starting *esg*<sup>+</sup> not proliferating cells



**E**  With co-dividing siblings  
 Without co-dividing siblings

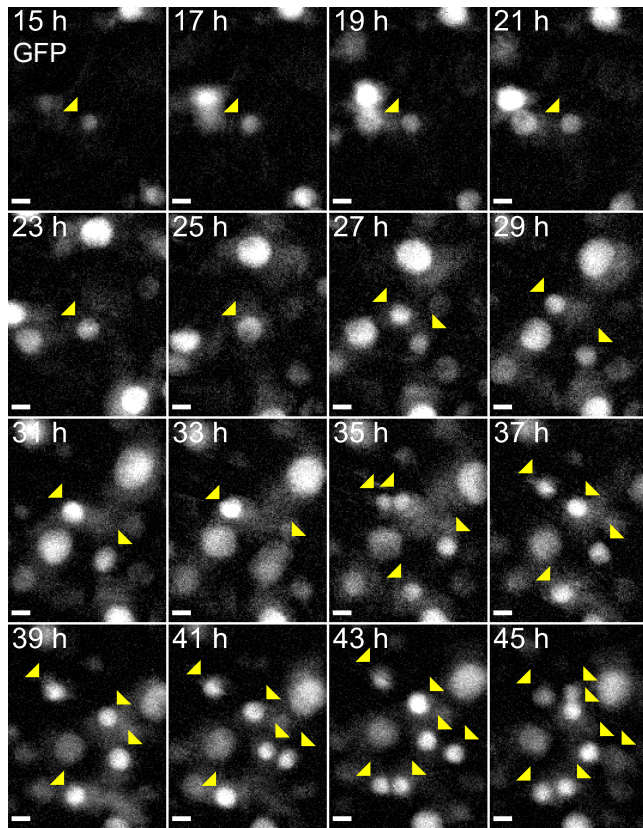


**F**

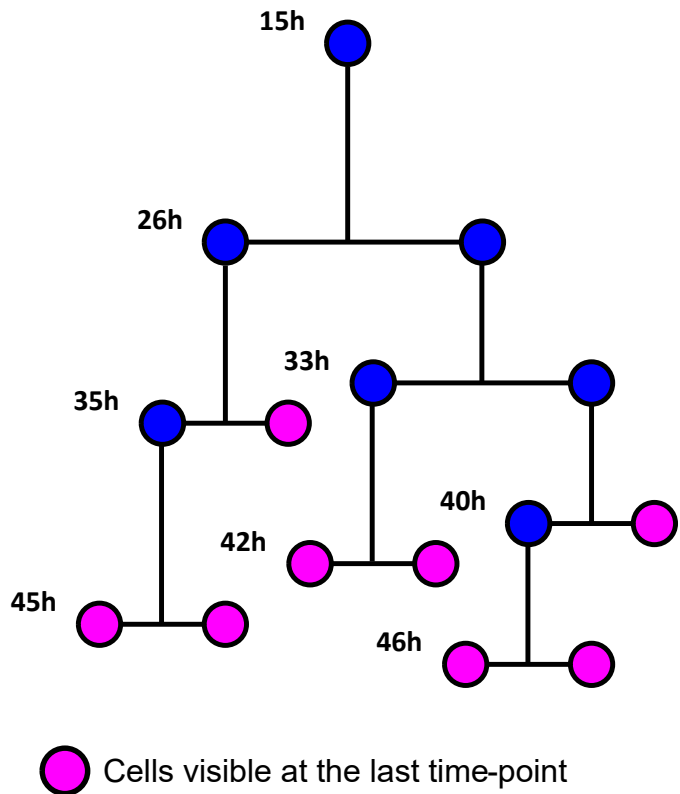


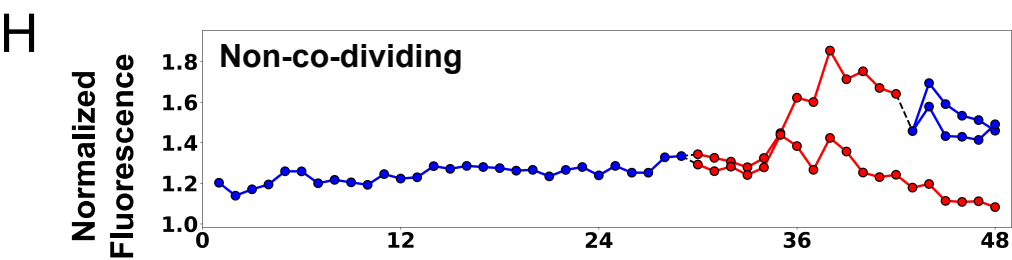
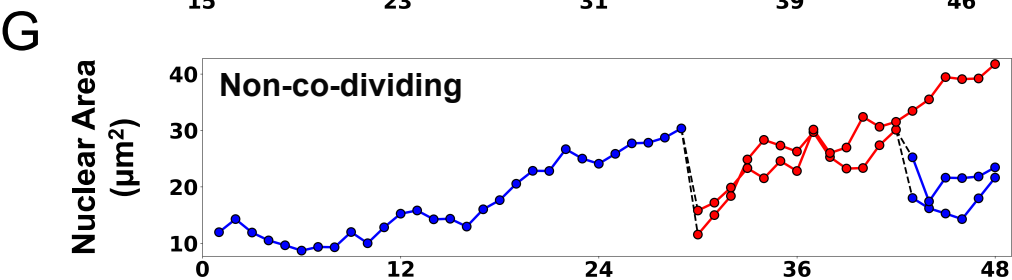
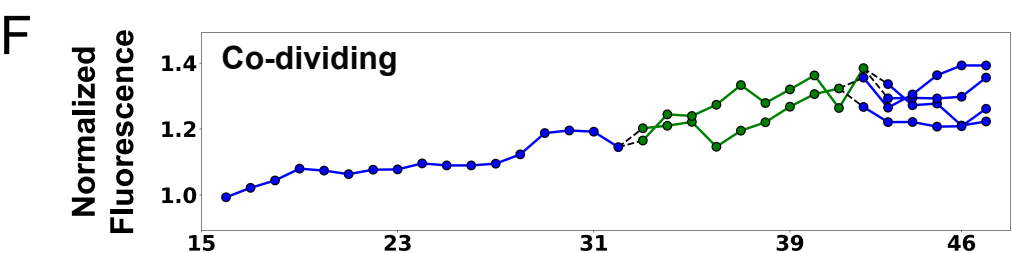
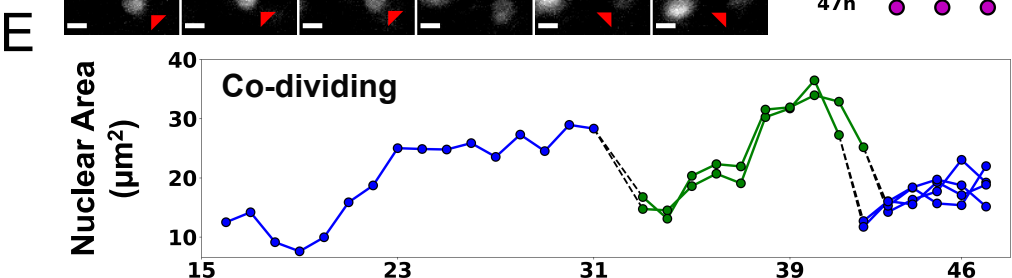
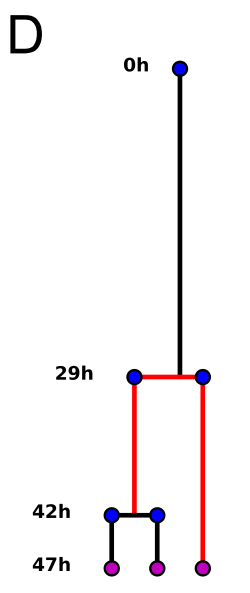
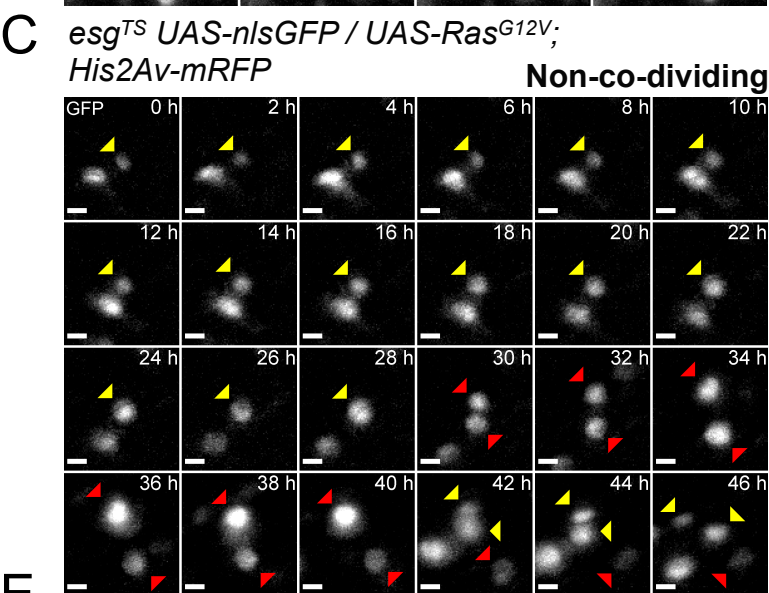
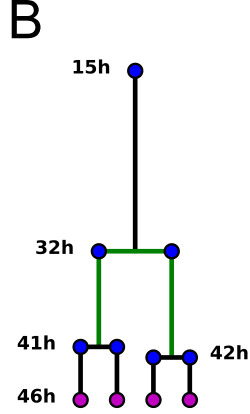
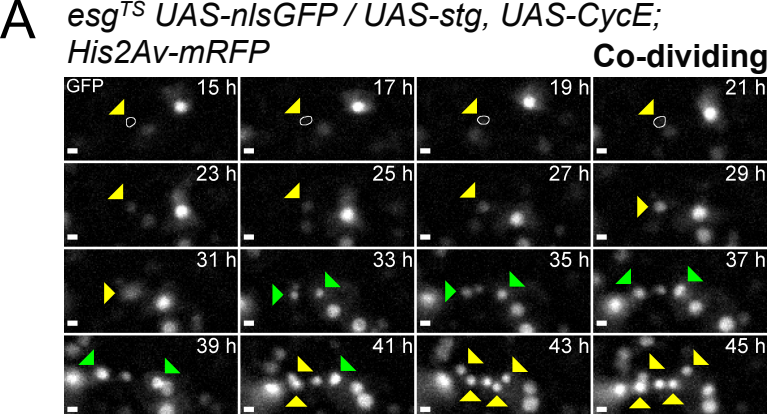


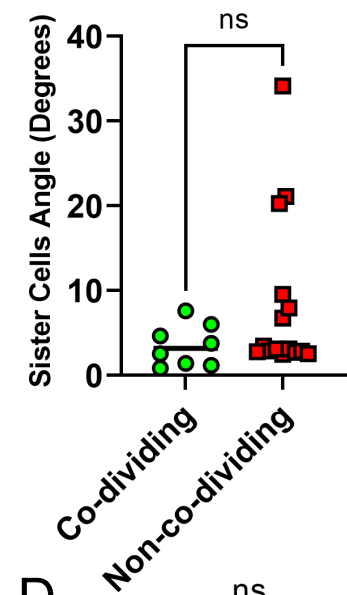
**A** *esg<sup>TS</sup> UAS-nlsGFP / UAS-Ras<sup>G12V</sup>;  
His2Av-mRFP*



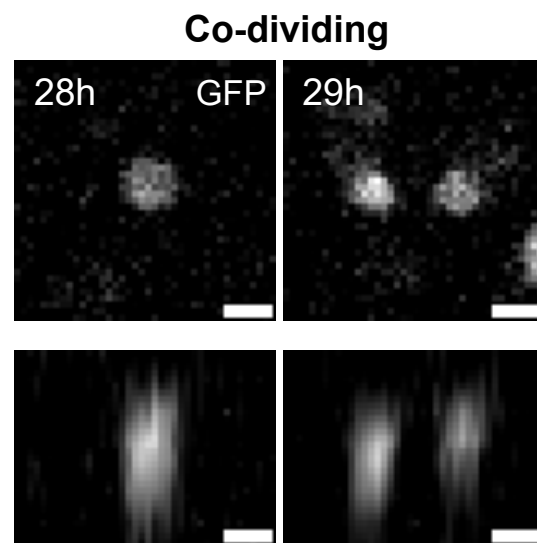
**B**



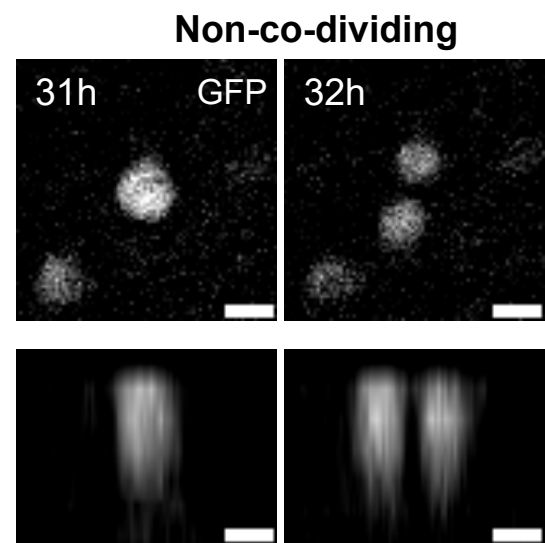
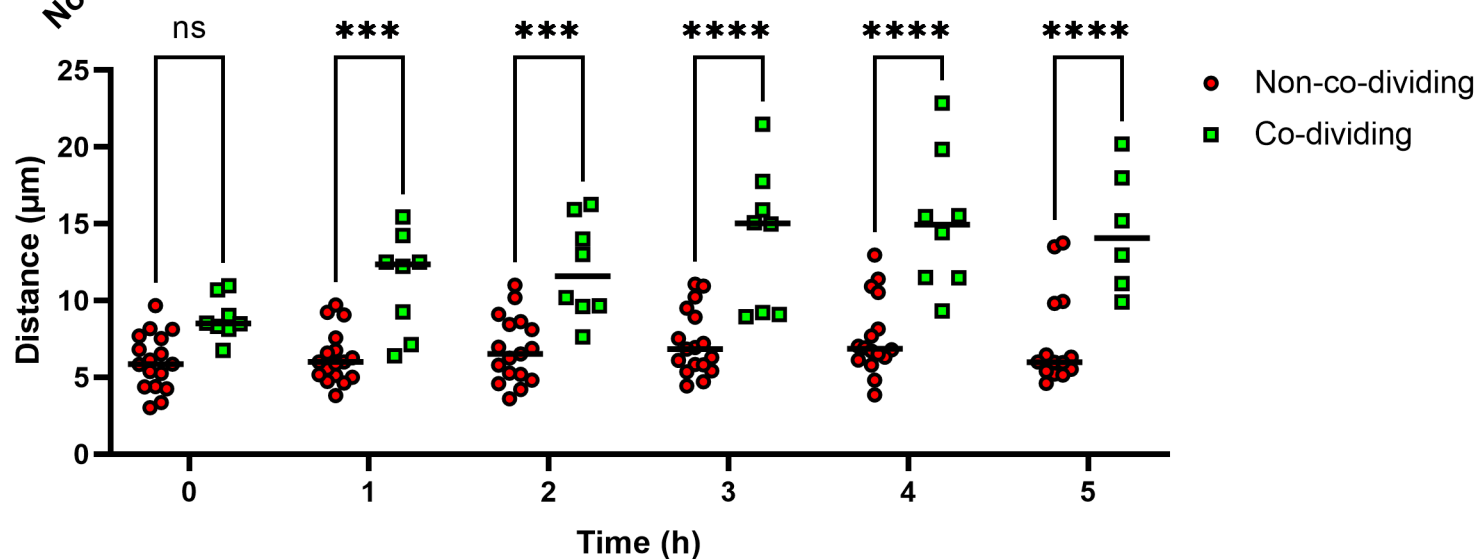


**A****B**

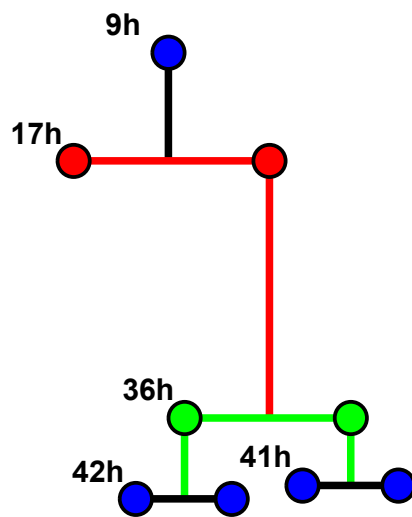
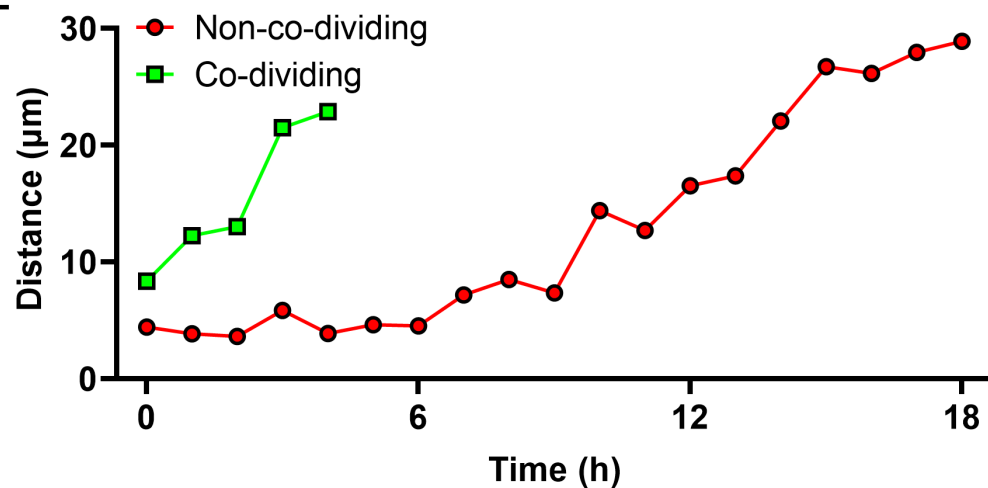
*esg<sup>TS</sup> UAS-nlsGFP / UAS-stg, UAS-CycE*  
*His2Av-mRFP*

**C**

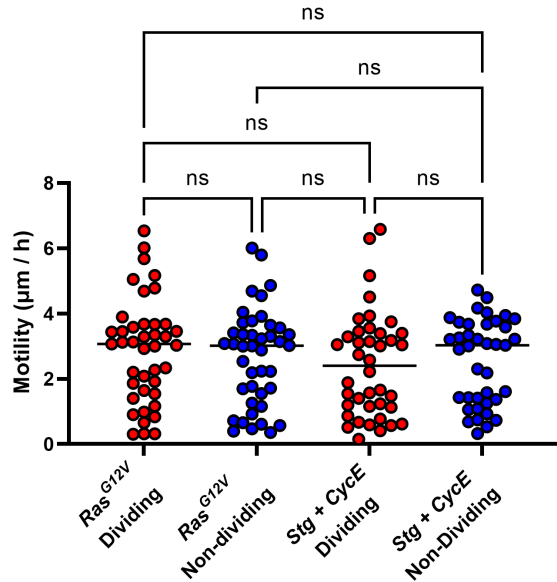
*esg<sup>TS</sup> UAS-nlsGFP / UAS-Ras<sup>G12V</sup>*  
*His2Av-mRFP*

**D****E**

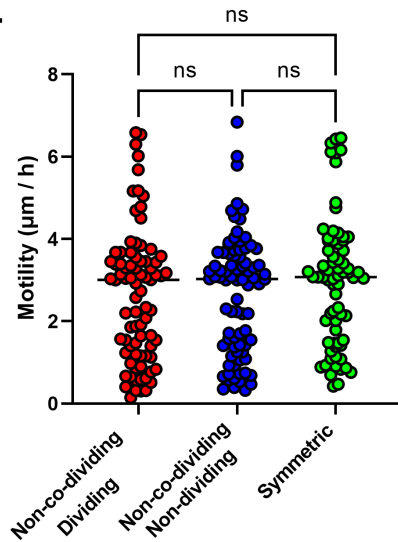
*esg<sup>TS</sup> UAS-nlsGFP / UAS-stg, UAS-CycE*  
*His2Av-mRFP*

**F**

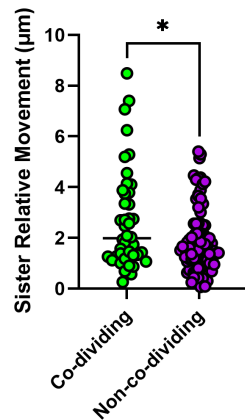
A



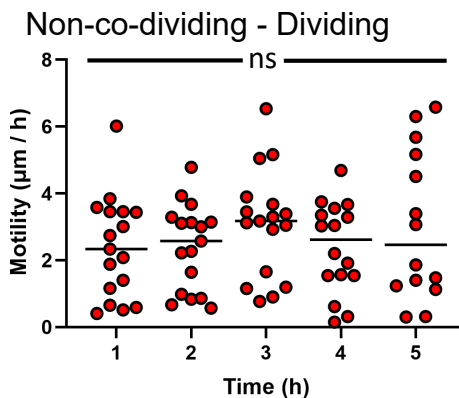
E



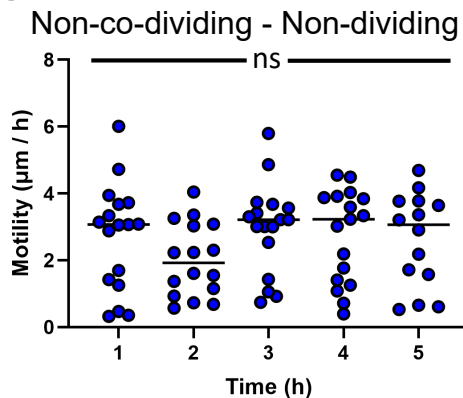
F



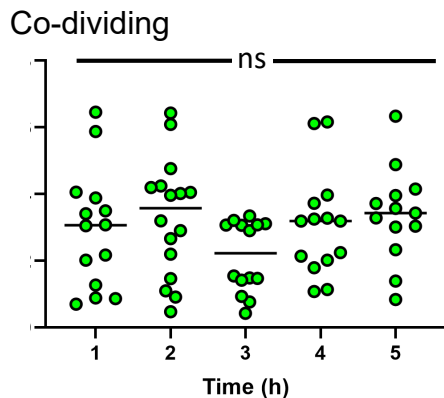
B



C



D



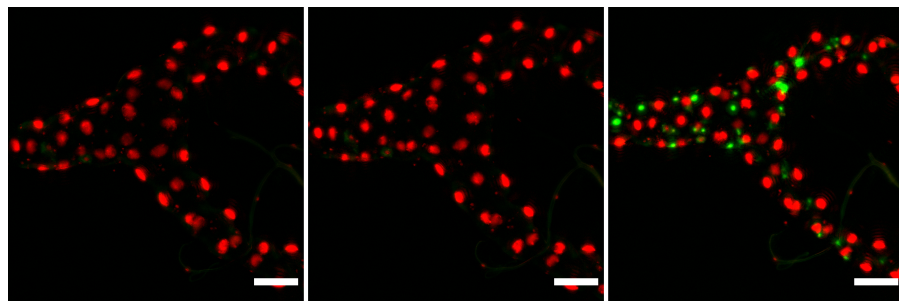
A

*esg-Gal4 Tub-GA/80<sup>TS</sup> UAS-*nlsGFP*;  
His2Av-*mRFP**

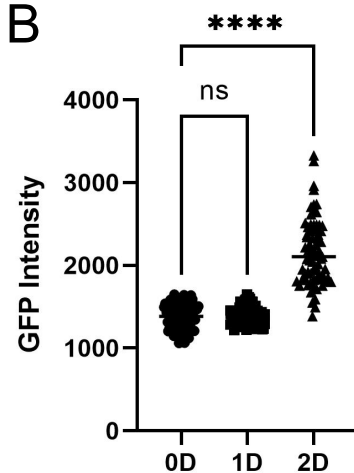
0h

24h

48h (24h @ 29C)

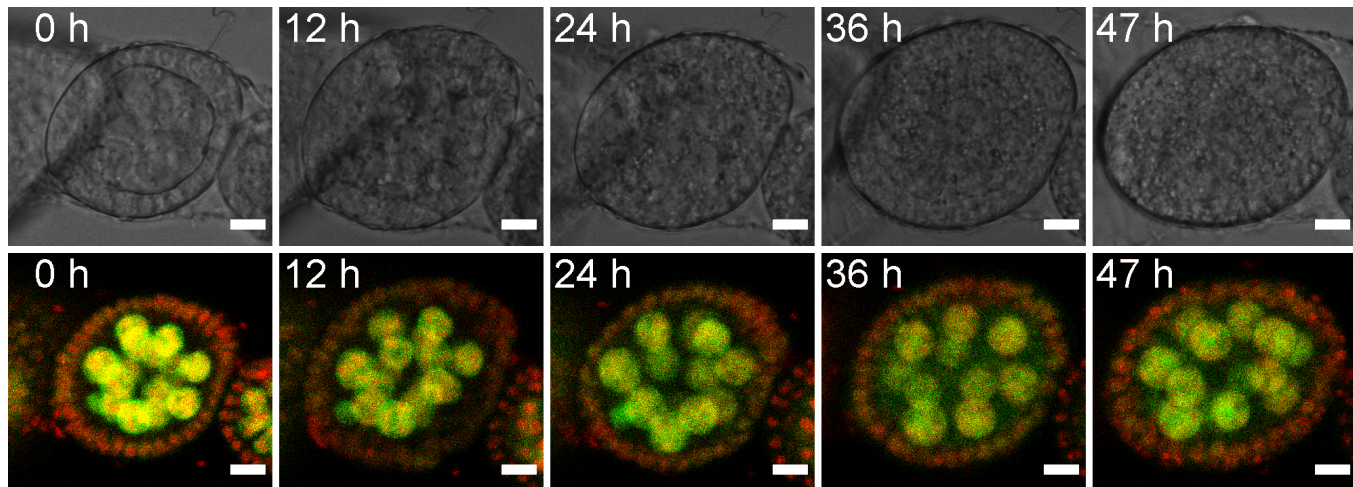


B



C

*His2Av-*mRFP*;  
PCNA-*GFP**



C'

